The versican-hyaluronan complex provides an essential extracellular matrix niche for Flk1+ precursors in vasculogenesis and primitive hematopoiesis

Sumeda Nandadasa, Anna O'Donnell, Ronald J. Midura and Suneel S. Apte*

Department of Biomedical Engineering (ND20), Cleveland Clinic Lerner Research Institute, 9500 Euclid Avenue, Cleveland, OH 44195

*Lead contact and corresponding author: Suneel S. Apte, MBBS, D.Phil., Department of Biomedical Engineering-ND20, Lerner Research Institute, Cleveland Clinic, 9500 Euclid Avenue, Cleveland, OH 44195, USA. Phone: 216.445.3278; E-mail: aptes@ccf.org

Summary

Extracellular matrix aggregates comprising the proteoglycan versican and glycosaminoglycan hyaluronan are necessary for cardiac development. Here we identify failure of primary vascular plexus formation and attenuation of primitive hematopoiesis in the yolk sac of the mouse insertional mutant *Vcan*^{hdf}, which lacks all versican isoforms. Spatially co-regulated versican and hyaluronan were intimately associated with Flk1+ hematovascular progenitor cells migrating from the primitive streak into extraembryonic mesoderm, although not with the differentiated successors. In the absence of versican, yolk sac and embryo hyaluronan were severely depleted, suggesting that versican stabilizes extracellular hyaluronan. *Vcan* inactivation by CRISPR/Cas9 in mouse embryonic stem cells reduced expression of vascular endothelial and hematopoiesis markers in embryoid bodies, which formed fewer and shorter vascular sprouts in response to $VEGF_{165}$ and fewer blood colonies. These findings, together with single-cell transcriptome data, suggest that versican-hyaluronan pericellular matrix provides a crucial niche for hematovascular progenitors immediately after their genesis at gastrulation.

KEYWORDS: Proteoglycan; extracellular matrix; hyaluronan; versican; glycosaminoglycan; hemtatopoiesis; vasculogenesis; angiogenesis; vascular endothelium; embryonic stem cell

Introduction

The first blood vessels in amniotes form *de novo* in the yolk sac prior to initiation of hemodynamic forces, indicating an in situ differentiation driven by their local environment, which includes extracellular matrix (ECM). This vasculogenic process is inextricably linked to primitive hematopoiesis, i.e., formation of the first erythroid and myeloid cells (Risau and Flamme, 1995), implying a close lineage relationship or continuum between vascular endothelium and primitive eythropoiesis. The necessary progenitor cells arise from mesoderm at gastrulation, migrate from the primitive streak, and aggregate in blood islands in the proximal extra-embryonic yolk sac on the seventh day of gestation (E7) in mouse embryos (Dzierzak and Speck, 2008; Ferkowicz and Yoder, 2005). Several transcription factors and soluble effectors of vasculogenesis and hematopoiesis have been identified; although ECM and products of ECM turnover are known as major regulators of angiogenesis (Red-Horse et al., 2007), their effect on the first endothelial cells formed, the precursors of those cells and early hematopoietic cells is as yet undetermined. Primordial germ cells, which migrate to the extraembryonic allantois, are accompanied by a protective “traveling niche” of steel factor/stem cell factor producing cells during their journey to the gonads (Gu et al., 2009). Whether an ECM niche such as a pericellular matrix surrounds or accompanies developing and migrating hematovascular progenitor cells is unknown.

ECM surrounds all mammalian cells, other than circulating blood cells, forming a distinct pericellular matrix in some cell types, as well as an interstitial matrix. It regulates cell behavior by modulating cell adhesion, migration and tissue mechanics, sequesters growth factors and cytokines, and is a source of bioactive fragments. Proteoglycans, which are composite ECM and cell-surface molecules with one or more glycosaminoglycan chains covalently attached to a core protein, participate in all these mechanisms. For example, chondroitin sulfate proteoglycans (CSPGs) such as versican, which are bulky and inherently anti-adhesive, regulate focal adhesion formation and inhibit cell migration (Mead et al., 2018; Perris et al., 1996; Yamagata et al., 1989). Heparan sulfate proteoglycans (HSPGs) sequester growth

factors, including angiogenic growth factors such as VEGF-A and FGF2 through heparan sulfate (HS) chains and act as co receptors for angiogenic signaling (van Wijk and van Kuppevelt, 2014). Although CSPGs can bind VEGF and functionally overlap with HSPGs in VEGF-induced sprouting angiogenesis (Le Jan et al., 2012), a physiological context for their VEGF-regulating activity has yet to be uncovered.

Versican is a widely distributed CSPG that aggregates with the glycosaminoglycan hyaluronan (HA), through its N-terminal G1 domain (Bode-Lesniewska et al., 1996; Kimata et al., 1986; Shinomura et al., 1993; Zimmermann and Ruoslahti, 1989). Its C-terminal G3 domain binds to ECM components fibronectin, fibrillins and tenascins (Wu et al., 2005) as well as VEGF-A (Zheng et al., 2004). Through interaction of HA with cell-surface receptors such as CD44, versican is a major component of pericellular matrix, where it regulates cell adhesion and consequently, contractile cytoskeleton assembly, and is postulated to influence cell differentiation through this mechanism (Hattori et al., 2011; Mead et al., 2018; Nandadasa et al., 2015). Four versican isoforms (V0, V1-V3) arise from alternative splicing of large exons, numbered 7 and 8, that encode the CS-bearing domains, named GAGα and GAGβ respectively (Dours-Zimmermann and Zimmermann, 1994; Shinomura et al., 1993). The versican insertional mutant mouse allele (*Vcan*^{Hdf}), which lacks all isoforms, identified an essential role for versican in early cardiac development (Mjaatvedt et al., 1998; Yamamura et al., 1997). Like *Vcan*$^{Hdf/Hdf}$ embryos, *Has2* null embryos, lacking the major HA synthase die by 10.5 days of gestation with similar cardiac defects (Camenisch et al., 2000), demonstrating that the versican-HA complex is a major constituent of cardiac jelly. Here, upon identification of an abnormal vasculature in *Vcan*$^{Hdf/Hdf}$ yolk sac, we investigated its role in vasculogenesis and early hematopoiesis. The analysis demonstrated intimate association of versican and HA with Flk1+ hematoendothelial progenitor cells from their origin at gastrulation, demonstrated that versican was necessary for retaining HA in embryonic ECM, and indicated a vital role for the versican-HA pericellular matrix in determining Flk1+ progenitor fate.

Results

Vcan$^{Hdf/Hdf}$ yolk sacs lack a vascular plexus:

Vcan$^{Hdf/Hdf}$ embryos did not survive past E10.5, and were readily distinguished at E9.5 by their small size and dilated pericardial sac (Fig. 1A). Although major developmental milestones, including chorio-allantoic fusion, neural pore closure, axial rotation of the embryo, formation of branchial arches and initiation of cardiac contraction, were completed appropriately by E9.5, *Vcan*$^{Hdf/Hdf}$ yolk sacs and embryos appeared substantially less vascular (Fig. 1B,C). Whole mount CD31 immunostaining revealed the absence of a vascular network in E9.5 *Vcan*$^{Hdf/Hdf}$ yolk sacs contrasting with a well-branched network in the wild type yolk sac. Instead, unorganized, scattered vascular endothelial cells were evident in *Vcan*$^{Hdf/Hdf}$ yolk sacs (Fig. 1C).

Immunostaining of E9.5 wild type yolk sac localized versican to ECM of yolk sac mesoderm where it surrounded the vasculature, whereas no staining was seen in wild-type visceral endoderm and *Vcan*$^{Hdf/Hdf}$ yolk sacs (Fig. 1D). Intriguingly, staining with hyaluronan binding protein (HAbp), which showed overlapping distribution of HA and versican in wild type yolk sac mesoderm, identified an unexpected loss of HA staining in *Vcan*$^{Hdf/Hdf}$ yolk sacs (Fig. 1D). Fibronectin immunostaining in contrast, showed increased staining in *Vcan*$^{Hdf/Hdf}$ yolk sacs, whereas collagen IV staining was unaffected (Fig. 1D), suggesting that loss of HA was not a consequence of global ECM reduction in the *Vcan*$^{Hdf/Hdf}$ yolk sacs. Similar to other mouse mutants lacking yolk sac vasculogenesis and hematopoiesis including *Has2*, *Itga5* and *Fn1*-null alleles (Camenisch et al., 2000; Francis et al., 2002), *Vcan*$^{Hdf/Hdf}$ yolk sacs consistently showed detachment of the mesoderm from visceral endoderm and few blood islands or blood cells were observed (Fig 1D, Fig. S2 A-C). They also consistently showed more intense endoderm F-actin staining compared to the wild type (Fig. 1 D, Fig. S2A), and rounded, rather than spindle-shaped nuclei in yolk sac mesothelium (Fig. S2B). Transmission electron microscopy (TEM), using a method that preserves cell-matrix interactions (Hunziker et al., 1983) showed complete

coverage of blood islands with vascular endothelium in wild type yolk sac and detached vascular endothelial cells with numerous membrane protrusions in *Vcan*$^{Hdf/Hdf}$ yolk sacs (Fig. S2C). Thus, versican is essential for proper yolk sac morphogenesis and function.

We traced the chronology of yolk sac development retrospectively to determine the genesis of yolk sac avascularity. In contrast to E9.5 embryos, E8.5 *Vcan*$^{Hdf/Hdf}$ embryos were developmentally indistinguishable from wild type embryos, although they appeared pale and their yolk sacs lacked a visible vascular network (Fig. 2B). CD31 immunostaining of whole mount E8.5 embryos identified severe, widespread attenuation of vasculature (Fig. 2B). In wild type yolk sac, *en face* CD31 staining demonstrated a honeycomb-like plexus, which was absent in *Vcan*$^{Hdf/Hdf}$ yolk sacs (Fig. 2C). Intriguingly, immunostaining of versican and CD31, together with HA-staining in E8.5 wild type yolk sacs revealed that versican and HA consistently co-localized in patches corresponding to individual endothelial cells on the mesothelial aspect of blood islands (Fig. 2D). RNA *in situ* hybridization with *Vcan* exon 7 (GAG α), or exon 8 (GAG β)-specific probes revealed that only the exon 8 probe hybridized to E8.5 yolk sac mesoderm (Fig 2E), suggesting prevalence of the versican V1 isoform at this developmental stage. In contrast, both *Vcan* probes hybridized strongly to E8.5 wild type hearts (Fig. 2F) and did not hybridize to *Vcan*$^{Hdf/Hdf}$ hearts (e.g., exon 8 probe, Fig. 2G), indicative of their specificity.

Versican and HA surround Flk1+ progenitor cells

Since *Vcan*$^{Hdf/Hdf}$ yolk sacs and embryos had defective vasculogenesis and few blood cells, we investigated the relationship between versican patches in the blood islands and hematovascular progenitor cells. Flk1, a well characterized hemo-endothelial progenitor marker, indispensable for both vascular and blood lineage development (Shalaby et al., 1997) showed complete overlap with versican and hyaluronan on the mesothelial aspect of blood islands in wild type E8.5 yolk sac (Fig. 3A). *Vcan*$^{Hdf/Hdf}$ yolk sacs, in contrast, showed small blood islands with dramatically attenuated HA and Flk1 staining (Fig. 3A). *En face* confocal microscopy of dissected E8.5 whole mount yolk sacs revealed discrete patches of versican distributed

throughout the mesoderm (Fig. 3B). CD41, which is expressed upon specific commitment to the blood lineage (Ferkowicz et al., 2003), was strongly expressed in blood islands in the mid-mesoderm plane in wild type yolk sacs (Fig. 3B). Versican did not colocalize with CD41+ cells and was restricted to intense patches corresponding to individual endothelial cells in wild type yolk sacs, evident both in the surface (mesothelial) plane and cross sections and *Vcan*$^{Hdf/Hdf}$ yolk sacs lacked CD41-stained blood islands entirely (Fig. 3B). High magnification images show a few cells with weak CD41 staining in *Vcan*$^{Hdf/Hdf}$ yolk sac mesoderm (arrowheads in Fig. 3B), contrasting with well-demarcated CD41+ wild-type blood islands. Combined, these results show that versican and HA distribution at E8.5 is restricted and specific to uncommitted Flk1+ hemogenic endothelial cells, which are crucial for both blood and vascular development in the mouse embryo. However versican and HA are not associated with blood cells through subsequent differentiation (Fig. 3B,C).

Methylcellulose colony formation assays demonstrated fewer colony-forming units (CFUs) in E8.5 *Vcan*$^{Hdf/Hdf}$ embryos and yolk sacs (Fig. 3D), in agreement with fewer CD41-stained blood islands observed in the yolk sac. Similarly, qRT-PCR revealed significantly lower *Flk1* expression in *Vcan*$^{Hdf/Hdf}$ yolk sac and embryos (Fig. 3E), in agreement with reduced Flk1 staining observed in situ in the mutant (Fig. 3A). Neither expression of *Has2*, encoding the major HA synthase in the embryo, nor of *Brachyury*, a mesoderm marker, were altered in *Vcan*$^{Hdf/Hdf}$ yolk sacs or embryos (Fig. 3F). Expression of genes encoding blood lineage commitment markers *Itga2b* (CD41) and *Runx1* were similarly reduced in the *Vcan*$^{Hdf/Hdf}$ yolk sacs and embryos (Fig. 3G), as well as erythroid and myeloid transcripts *Hbb* (β-globin), *Gata1* and *Ptprc* (CD45) (Fig. 3H). CD31 (*Pecam1*) mRNA expression was greatly reduced in the *Vcan*$^{Hdf/Hdf}$ yolk sacs and embryos (Fig. 3I), consistent with the observed lack of vasculature (Fig. 2B). These data suggested that lack of the versican-HA resulted in impaired blood and vascular differentiation.

Versican and HA are associated with Flk1 cells at gastrulation

Since Flk1+ cells arise at gastrulation, we analyzed versican and HA localization in wild type E7.5 mouse embryos. Strikingly, versican staining of whole mount E7.5 embryos revealed ring-like distribution in the proximal extraembryonic region coinciding with the expected location of the blood island ring (Fig. 4A). Sections from these embryos demonstrated versican and HA co-localization in the extraembryonic mesoderm in the blood island region (Fig. 4B). Confocal microscopy revealed that the versican-HA patches corresponded to the location of Flk1+ mesodermal progenitor cells (Fig. 4C,D). RNA *In situ* hybridization of serial sections from several embryos showed considerable overlap between *Vcan* exons 7 and 8, *Has2* and *Flk1* expressing cells in extraembryonic mesoderm and embryonic mesoderm (Fig. 4E, Fig. S3). *Vcan* exon 7-containing transcripts showed less intense expression than exon 8 probes in the blood island ring, although they were detected. *Runx1*, which specifically defines blood lineage-committed cells, was expressed by cells in a region of proximal extraembryonic mesoderm distinct from that expressing *Flk1*, *Vcan* and *Has2* (Fig. 4E, Fig. S3). Thus, these data localize versican and HA to a hematovascular compartment defined by Flk1+ cells and suggest that a versican-HA ECM is intimately associated with and a defining characteristic of Flk1+ cells.

Data mining of a recently published single cell RNA sequencing (scRNAseq) analysis of the early mouse embryo spanning gestational ages 6.5 to 8.5 days (Pijuan-Sala et al., 2019) provided further insights on the association of versican with hemato-endothelial progenitors. High *Vcan* expression was first detected in hematoendothelial progenitors emerging at E6.75, as well as in nascent and uncommitted mesoderm (Fig. 5A-C). The data showed strong *Vcan* expression in *Kdr*-expressing cells (Flk1+ cells) at E6.75, E7.0 and E7.5, spanning mouse gastrulation (Fig. 5A-C). *Kdr*+ cells also expressed *Has2*, encoding the major embryonic hyaluronan synthase, and the gene encoding a major hyaluronan receptor, CD44 (Fig. 5B). These observations further support a cell autonomous role for versican, bound to HA and thus to the cell surface by CD44 and Has2, which forms a membrane channel spooling out HA, and acts as a *de facto* HA receptor. Notably, since versican is secreted, its expression in the vicinity

of cells expressing CD44 or HA could also lead to incorporation into pericellular ECM of the latter. After E7.5, e.g., at E 8.5, *Vcan* expression is less restricted, occurring in mesoderm, the developing brain, allantois and cardiomyocytes (Fig. 5A,C) and *Kdr* expression extends into endothelial cells. Nevertheless, subsequent hematoendothelial progenitors continue to express *Vcan*.

Loss of versican dramatically reduces yolk sac and embryo HA levels

In addition to reduced HA in yolk sac blood islands in the absence of versican, we identified a dramatic loss of HAbp staining throughout *Vcan*$^{Hdf/Hdf}$ embryos (Fig. 6A). *Has2* mRNA expression was unaltered in *Vcan*$^{Hdf/Hdf}$ embryos and yolk sacs (Fig. 3F). Since reduced HAbp staining could result from extraction of unliganded HA from *Vcan*$^{Hdf/Hdf}$ tissue sections during the staining process, fluorophore-assisted carbohydrate electrophoresis (FACE) (Calabro et al., 2000a; Calabro et al., 2000b; Midura et al., 2018) was undertaken on snap-frozen whole embryos (Fig. 6B-D). FACE analysis provided several interesting observations: First, versican is the major CSPG in the E8.5 embryo, contributing nearly all the unsulfated (0S) forms of CS, since both the overall level of CS and its 0S form were dramatically reduced in *Vcan*$^{Hdf/Hdf}$ embryos (Fig. 6B). In addition, the data clearly showed reduction of total HA compared to wild type littermates (Fig. 6C-D). In combination with unaltered *Has2* levels, these findings suggest increased turnover of HA in the absence of versican. Consistent with reduced versican and HA, craniofacial mesenchyme and myocardium were considerably compacted in the absence of versican (Fig. 6E,F). We also asked whether the absence of versican affected fibronectin, a major embryonic ECM component that is essential for angiogenesis and observed a dramatic increase both in fibronectin staining and mRNA in *Vcan*$^{Hdf/Hdf}$ embryos (Fig. 6G-I). Thus, both *Vcan*$^{Hdf/Hdf}$ yolk sac and embryo demonstrate a reduction of HA and excess fibronectin.

Embryoid bodies formed by *Vcan*-null ES cells have impaired angiogenesis and hematopoiesis.

Although these data strongly suggest a local role for a versican-HA pericellular ECM in hemato-endothelial progenitors emerging at gastrulation, a lack of hemodynamic forces arising from the cardiac defect in *Vcan*$^{Hdf/Hdf}$ embryos may influence the dramatic loss of vasculature seen later in embryogenesis (E8.5-9.5). To investigate the role of versican independent of heart development, we used gene editing by CRISPR/Cas9 (Doudna and Charpentier, 2014; Jinek et al., 2012) to introduce *Vcan*-null mutations in R1 mouse embryonic stem (mES) cells (Nagy et al., 1993). *Vcan* exon 2 (containing the start codon) and exon 3 (start of the G1 domain) were targeted independently to obtain mES cell clones D8 and F9 respectively, each with defined frameshift mutations that generate null alleles (Fig. 7A). Since exons 2 and 3 are included in all *Vcan* splice isoforms, no versican was produced, as shown by western blot with anti-GAGβ antibody (Fig. 7B). The mutated clones retained normal expression of *Oct4, Sox2, Nanog* and *C-myc* (Fig. 7C) indicating their pluripotency was unaffected by *Vcan* mutagenesis, and validating their suitability for *in vitro* differentiation. *Vcan*-null and wild-type ES cells were allowed to dedifferentiate and form embryoid bodies (EBs), in which random differentiation into various lineages occurs. RT-qPCR analysis of *Has2* showed no change in *Vcan*-null EBs (Fig. S4A) while the mesoderm differentiation marker *Brachyury/T* showed a significant decrease in the F9 but not the D8 *Vcan*-null EBs (Fig. S4B). Similar to *Vcan*$^{Hdf/Hdf}$ embryos, *Vcan* null embryoid bodies showed reduced expression of *Flk1* (Fig. S4C), and the blood lineage commitment markers *Itga2b* (CD41) and *Runx1* (Fig. S4D), as well as differentiated-blood and vascular endothelial markers (Fig. S4E, F). Since EB differentiation is random and unaccompanied by formation of a closed circulation, the data strongly suggest that versican acts directly on Flk1+ hematoendothelial progenitors rather than indirectly via its role in cardiac development. In addition, *Vcan* null EBs demonstrated spontaneous rhythmic contractions suggesting unimpaired differentiation to cardiomyocytes (Supplemental Movie).

To further evaluate the impact on hematoendothelial progenitors, we separately evaluated endothelial and hematopoietic potential. Sprouting angiogenesis was induced by

culturing 4-day differentiated EBs in 3-dimensional collagen I gels and treatment with VEGF-A_{165} for 12 days (Baker et al., 2012). Following VEGF stimulation, robust angiogenic sprouting identified by CD31 and smooth muscle α-actin staining was seen in wild-type EBs, but not in the majority of *Vcan*-null EBs (Fig. 7D,E). The few *Vcan*-null EBs with sprouting had fewer sprouts per EB, and these were significantly shorter than wild type sprouts (Fig. 7F,G). When 10-day old EBs were disaggregated and the cells were plated in a 3-dimensional methylcellulose matrix containing a complete set of blood differentiation cytokines, significantly fewer blood colonies were formed by *Vcan* null EBs (Fig. 6H).

Discussion

Although versican is widely expressed during organogenesis and in adult tissues (Bode-Lesniewska et al., 1996), a notable finding of this work is its specific association with Flk1+ cells from their earliest origin from the mesoderm until establishment of yolk sac vasculature and primitive hematopoiesis. Furthermore, analysis of both *Vcan* mutant mice *in vivo* and *Vcan*-null embryoid bodies *in vitro* suggest that versican has an essential role in vasculogenesis and primitive hematopoiesis. Taken together, the RNA in situ hybridization data, scRNAseq analysis of Flk1+ cells, and immunostaining of embryos suggests that versican is a product of Flk1+ cells that associates with them via HA and CD44 to form a pericellular matrix. Another major finding of this study is a substantial loss of embryonic and extraembryonic HA in the absence of versican.

As in *Vcan*$^{Hdf/Hdf}$ yolk sac, avascularity was previously noted in *Has2* null yolk sac (Camenisch et al., 2000), although it was not studied further. *Has2* and *Vcan* null cardiac defects are similar, which suggested that an obligate versican-HA complex in cardiac jelly and endocardial cushions was required for cardiac morphogenesis (Camenisch et al., 2000; Mjaatvedt et al., 1998; Yamamura et al., 1997). Thus, a versican-HA complex, rather than versican alone, is necessary for vasculogenesis and primitive hematopoiesis, forming a pericellular ECM that constitutes a niche for Flk1+ cells and promotes their survival or

differentiation to endothelial and blood cells (Fig. 7). HA-versican aggregates have a net negative charge, and swelling via absorption of water (the Gibbs-Donnan effect) (Buschmann and Grodzinsky, 1995). As shown here and previously, tissues compact in their absence (Mjaatvedt et al., 1998; Szabo et al., 2016). Although versican-deficient yolk sac showed extensive structural disorganization at E9.5, it is clear that the association and effect of versican vis-à-vis Flk1+ cells occurs much earlier, i.e., shortly after gastrulation. Reduced vasculogenesis, angiogenesis and hematopoiesis in embryoid bodies argues also against a secondary effect of a cardiac defect on vasculogenesis, as well as against yolk sac disorganization at E9.5 having a major primary impact on blood island formation. We therefore conclude that versican-HA aggregates act directly and as early as E6.75 within the microenvironment of Flk1+ cells.

Versican and HA form a pericellular matrix in fibroblasts and vascular and myometrial smooth muscle cells (Evanko et al., 1999; Hattori et al., 2011; Mead et al., 2018) which is influential in determining cell phenotype. Specifically, HA, which is extruded from HAS2 complexes in the cell membrane, is decorated with versican and the complex is retained at the cell surface by binding CD44, HAS2 and other receptors (Evanko et al., 2007). *Cd44* is coordinately expressed with *Vcan* and *Has2* in hematoendothelial progenitor cells. *Cd44* null mice survive and are not known to have vasculogenesis of primitive erythropoiesis defects (Protin et al., 1999), suggesting that other HA receptors may participate. The versican-HA pericellular matrix has a well-established impact on different cells. It is anti-adhesive (Evanko et al., 1999; Mead et al., 2018), which may allow the Flk1+ cells to migrate and proliferate efficiently after their emergence at gastrulation. Another possible role of versican-HA is sequestration of vasculogenic factors such as VEGF-A. Versican binding to VEGF-A via its CS-chains (Le Jan et al., 2012) or G3 domain (Zheng et al., 2004), may generate high concentrations around Flk1+ cells (Fig. S7). Versican is associated with Flk1+CD41- cells at their origin, but not with the Flk1-CD41+ yolk sac cells that arise subsequently suggesting that

the versican-HA pericellular ECM specifically regulates the fate of Flk1+ cells. We propose that as the dominant CSPG in the embryo, specifically localized to the pericellular ECM of Flk1+ cells, versican may sequester essential trophic factors such as VEGF-A to provide a high local concentration that sustains the Flk1+ population.

Although versican and HA immunostaining (each detecting secreted molecules) strongly labels the blood island ring, their mRNA expression begins in the migratory phase when the progenitor cells first arise from the primitive streak. Alternatively, deposition by neighboring Flk1- mesoderm may commence prior to the progenitor cells taking up residence in blood islands. Because of the dynamic migration of these cells after gastrulation, it may be challenging to ascertain whether the cells move through a versican-HA matrix or carry it with them as an autonomous pericellular matrix. Curiously, and presently unexplained, lack of versican led to more intense *Fn1* expression. The observed *Vcan*-deficient defects are unlikely to result from excess fibronectin, because previous work has shown that deficiency, not excess of fibronectin or the fibronectin receptor subunit α5 integrin results in reduced embryo and yolk sac vascularity (Francis et al., 2002; George et al., 1993). Taken together with the finding that versican binds fibronectin through the G3 domain (Zheng et al., 2004), we conclude that the three major components of the provisional embryonic ECM (versican, HA and fibronectin) are each crucial for establishment of the first blood vessels in the embryo. In the absence of versican, the HA catabolism rate likely exceeds the HA anabolism rate since *Has2* mRNA levels were relatively unchanged. It was previously noted that HA deposition was reduced to 85% of normal in fibroblasts from a mouse hypomorphic *Vcan* mutant ($Vcan^{\Delta 3/\Delta 3}$) with 75% reduction of versican (Suwan et al., 2009). Accompanying reduced HA deposition, $Vcan^{\Delta 3/\Delta 3}$ fibroblasts had accelerated senescence, suggesting a possible mechanism for the lack of Flk1+ cells in $Vcan^{Hdf/Hdf}$ yolk sac.

We found a stronger association of exon 8-containing *Vcan* transcripts than exon 7-containing transcripts with blood islands at gastrulation and exon 7 transcripts were absent at

E8.5. Autosomal dominant splice site mutations affecting exon 8 (leading to its exclusion) and exon 8 deletions in humans cause Wagner syndrome (Kloeckener-Gruissem et al., 2006; Kloeckener-Gruissem et al., 2013; Rothschild et al., 2013), which is characterized by impaired vision and defects of the ocular vitreous and retina, but lacks consistent extra-ocular manifestations. Exon 7 inactivation in mice led to specific neural anomalies and subtle cardiac anomalies (Burns et al., 2014; Dours-Zimmermann et al., 2009). Thus, neither individual exon mutation in mice or humans is associated with embryonic lethality, defective vasculogenesis or impaired hematopoiesis. We conclude that both exon 7 and exon 8-containing transcripts, possibly including V0, the transcript containing both exons, are required for vasculogenesis and hematopoiesis.

The GAGβ domain encoded by exon 8 has a unique N-terminal sequence, which is cleaved by ADAMTS proteases at the E^{441}-A^{442} peptide bond in several contexts, notably cardiac valve development, interdigital web regression, umbilical cord development, neural tube and palate closure and myometrial activation (Mead et al., 2018; Nandadasa et al., 2014; Nandadasa et al., 2015). The resulting N-terminal versican V1 fragment, G1-DPEAAE^{441}, named versikine is bioactive in interdigital web regression and myeloma growth (Hope et al., 2016; McCulloch et al., 2009). A *Vcan* knock-in mouse mutant in which E^{441}-A^{442} was mutated to render it uncleavable has normal yolk sac avascularity (Nandadasa et al., manuscript in preparation), suggesting that E^{441}-A^{442} cleavage is not involved in hematovascular development.

In relation to the pro-vasculogenic role of versican-HA complexes, recent work found that syngeneic B16-F10 tumors in adult *Vcan*$^{Hdf/+}$ mice had significantly impaired angiogenesis and reduced growth (Asano et al., 2017). Relevant to the overlap of versican-HA with Flk1 expression, a recent study utilizing the same cancer model in *Flk1*+/- mice also found reduced angiogenesis during tumor growth (Oladipupo et al., 2018). Indeed, versican-HA matrix may have a broad role in formation of vasculature in a variety of physiological and disease settings.

Acknowledgments

This work was supported by the NIH-NHLBI Program of Excellence in Glycosciences award HL107147 (to S.S.A., R.J.M.,) and by the Allen Distinguished Investigator Program, through support made by The Paul G. Allen Frontiers Group and the American Heart Association (to S.S.A), the David and Lindsay Morgenthaler Postdoctoral Fellowship and the Mark Lauer pediatric research grant (to S.N.). Purchase of the Leica SP8 confocal microscope was supported by NIH SIG grant 1S10RR026820-01. We thank Dr. David LePage and Dr. Ron Conlon at the CWRU transgenic core for R1 mES cells, Eric Schultz and Joseph Gerow of the LRI Flow Cytometry Core for mES cell sorting, Valbona Cali for FACE assays, Dr. Judy Drazba and Mei Yin of the LRI Imaging Core for guidance with confocal and electron microscopy and the Apte laboratory members for valuable discussions.

Author contributions

S.N. and A.O conducted experiments. S.N., R.J.M., and S.S.A. conceived experiments and interpreted the data. S.N. and S.S.A. wrote the paper. All authors read and edited the paper.

Declaration of interests

The authors declare no competing interests

Figures and Figure Legends

Figure 1

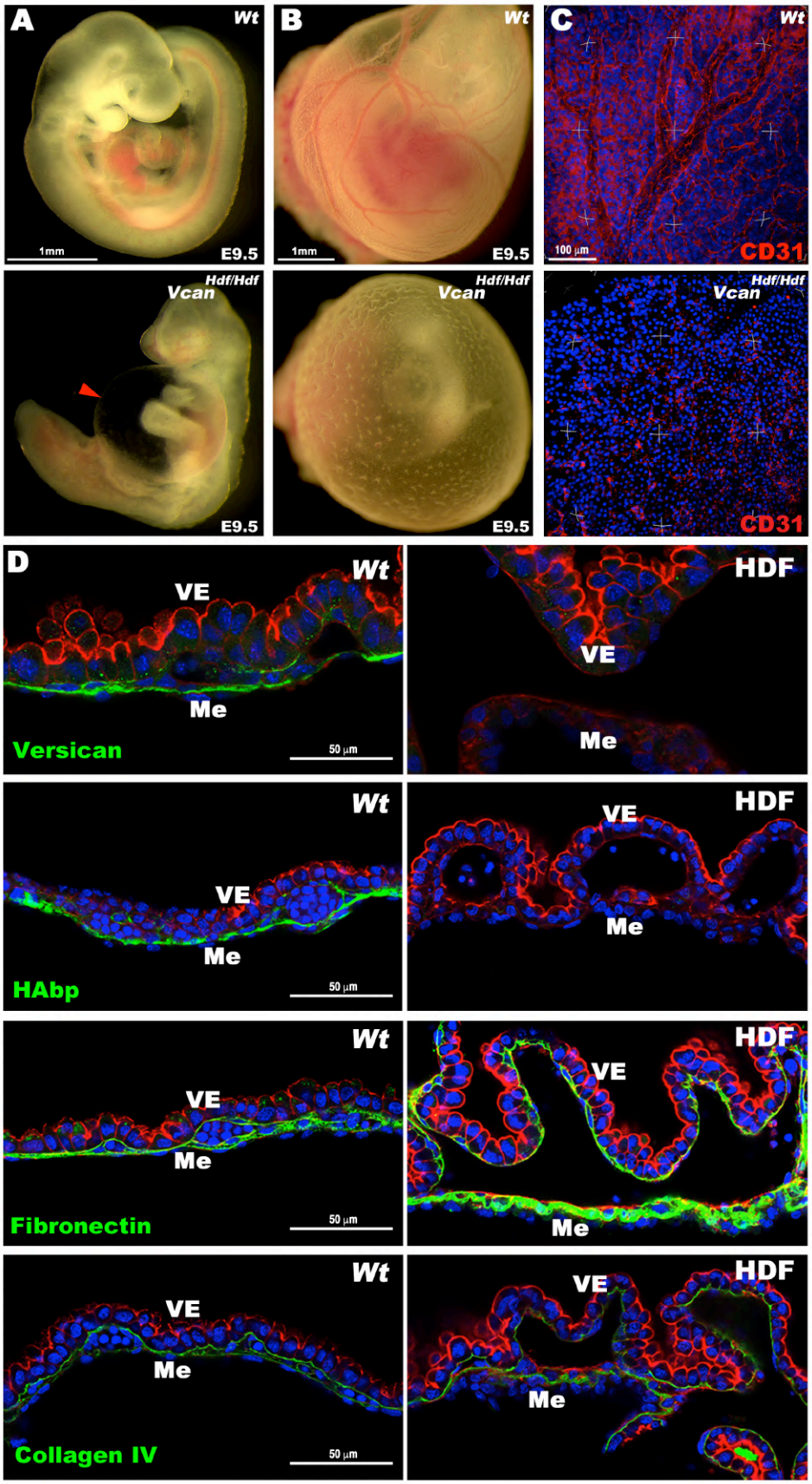

Figure 1. *Vcan*$^{Hdf/Hdf}$ yolk sacs are avascular and lack hyaluronan.

(A) E9.5 wild type and *Vcan*$^{Hdf/Hdf}$ embryos. The red arrowhead shows the dilated pericardial sac in the latter.

(B) E9.5 yolk sacs imaged in situ demonstrates the absence of vasculature in the E9.5 *Vcan*$^{Hdf/Hdf}$ yolk sac.

(C) Three-dimensional (3D) maximum intensity projections of whole mount yolk sacs stained with anti-CD31 (red) showing the absence of a vascular network in E9.5 *Vcan*$^{Hdf/Hdf}$ yolk sacs (N=3 yolk sacs of each genotype).

(D) Versican GAGβ staining (green) is present throughout the mesoderm (Me) of E9.5 wild type yolk sacs and absent in the *Vcan*$^{Hdf/Hdf}$ yolk sac. F-actin (red) staining highlights visceral endoderm (VE), which detached from the mesoderm in *Vcan*$^{Hdf/Hdf}$ yolk sac. HA and fibronectin (green) had a similar distribution as versican in wild type yolk sac, but HA staining was lost in *Vcan*$^{Hdf/Hdf}$ yolk sac, whereas fibronectin staining was more intense. Collagen IV staining intensity was similar in wild type and *Vcan*$^{Hdf/Hdf}$ yolk sacs (N=3 yolk sacs of each genotype). Scale bar in A,B=1mm, C= 100μm, D= 50μm.

Figure 2

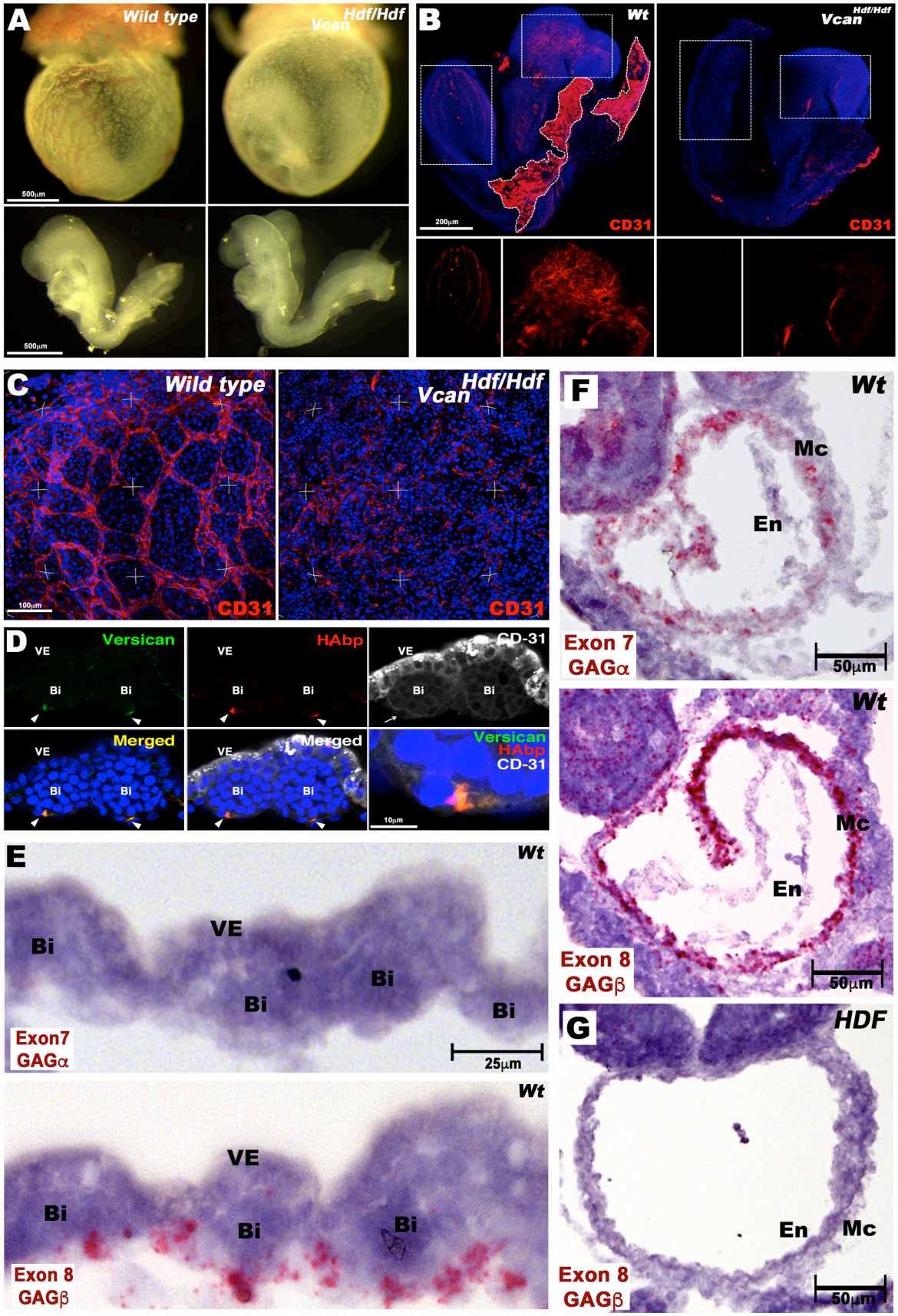
A
Wild type
Vcan Hdf/Hdf
500µm
500µm
B
Wt
Vcan Hdf/Hdf
200µm
CD31
CD31
C
Wild type
Vcan Hdf/Hdf
100µm
CD31
CD31
D
Versican
HAbp
CD-31
Merged
Merged
Versican
HAbp
CD-31
VE
Bi
10µm
E
Wt
VE
Bi
Exon7
GAGα
25µm
Wt
VE
Bi
Exon 8
GAGβ
F
Wt
Mc
En
Exon 7
GAGα
50µm
Wt
Mc
En
Exon 8
GAGβ
50µm
G
HDF
En
Mc
Exon 8
GAGβ
50µm

Figure 2. Impaired vasculogenesis in the *Vcan*$^{Hdf/Hdf}$ embryo and yolk sac.

(A) E8.5 *Vcan*$^{Hdf/Hdf}$ yolk sacs appear avascular whereas dissected embryos are morphologically similar to wild type.

(B) Maximum intensity projections of whole mount E8.5 wild type and *Vcan*$^{Hdf/Hdf}$ embryos stained with anti-CD31 (red). Boxed areas are shown at higher magnification without DAPI signal (blue) in the lower panels. Residual wild-type yolk sac tissue is marked by a white dotted line (N=3 embryos from each genotype).

(C) Three-dimensional (3D) maximum intensity projections of yolk sacs stained *en face* with anti-CD31 (red) showing a vascular plexus in wild type yolk sac and only unorganized CD31+ cells in *Vcan*$^{Hdf/Hdf}$ yolk sac (N=3 yolk sacs from each genotype).

(D) Cross section of E8.5 wild type yolk sac blood islands co-stained with versican (green), HAbp (red) and CD31 (white). Versican and HA co-localize to CD31+ cells on the mesothelial aspect of each blood island (arrowheads). The blood island imaged on the left is shown at higher magnification in the bottom right-hand panel (N=3 wild type yolk sacs). VE, visceral endoderm, Bi, blood island,

(E) RNAscope in situ hybridization of E8.5 wild-type yolk sac shows expression of *Vcan* isoforms containing exon 8 (V1), but not exon 7 (V0, V2) in mesoderm adjacent to blood islands (Bi), VE, visceral endoderm.

(F) *Vcan* exon 7 and exon 8 probes both hybridize to myocardium (Mc) of E8.5 wild-type embryos. En, Endocardium.

(G) *Vcan* exon 8 probe does not hybridize to *Vcan*$^{Hdf/Hdf}$ heart. Scale bar in D=10μm, E= 25μm, 50μm in F-G.

Figure 3

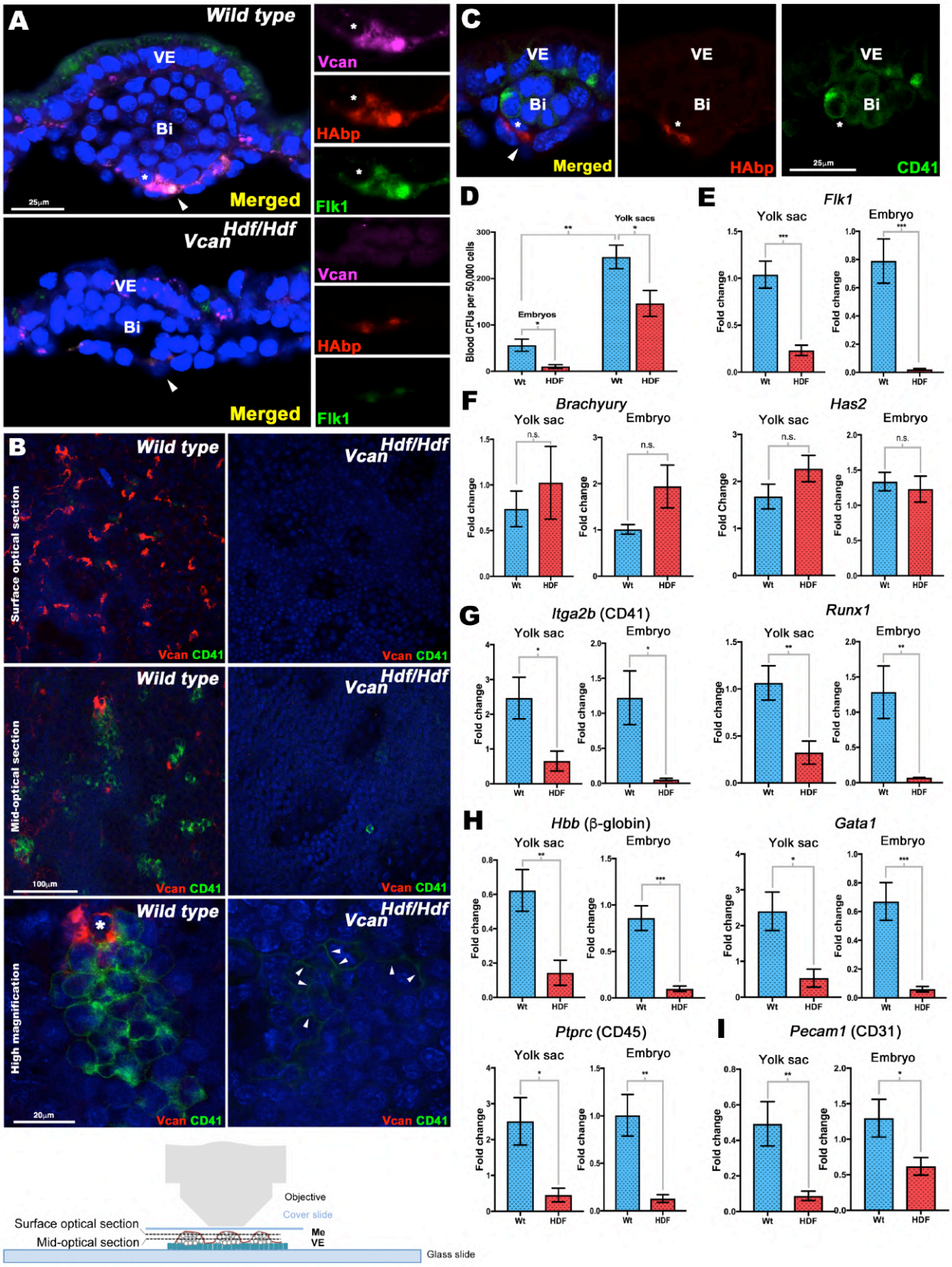
A
Wild type
VE
Bi
Merged
Vcan
HAbp
Flk1
Vcan Hdf/Hdf
B
Surface optical section
Mid-optical section
High magnification
Vcan CD41
C
D
Blood CFUs per 50,000 cells
Yolk sacs
Embryos
Wt
HDF
E
Flk1
Yolk sac
Embryo
Fold change
F
Brachyury
Has2
n.s.
G
Itga2b (CD41)
Runx1
H
Hbb (β-globin)
Gata1
Ptprc (CD45)
I
Pecam1 (CD31)
Objective
Cover slide
Surface optical section
Mid-optical section
Me
VE
Glass slide

Figure 3. Versican and HA localize to Flk1+ cells and are essential for yolk sac blood island formation.

(A) E8.5 wild type and *Vcan*$^{Hdf/Hdf}$ yolk sac cross-sections co stained with versican (magenta), HAbp (red) and Flk1 (green). In wild type yolk sac versican-HA staining colocalizes with Flk1. In *Vcan*$^{Hdf/Hdf}$ yolk sac, blood islands (Bi) are smaller and both HAbp staining and Flk1 staining are weak. The arrowhead shows versican-HA-Flk1 co-stained patches and asterisks mark a cell shown in high magnification in the right-hand panels (N=4 yolk sacs from each genotype). VE, visceral endoderm.

(B) *En face* confocal imaging of E8.5 yolk sac stained for versican (red) and CD41 (green). The sections were mounted with their mesothelial aspect facing the objective as shown at the bottom. Surface optical sections show versican-rich loci scattered throughout the wild type yolk sac that are absent in *Vcan*$^{Hdf/Hdf}$ yolk sac. The mid-optical plane shows both versican and CD41 stained cells in blood islands. A patch of versican is associated with each blood island but does not overlap with CD41+ cells. No CD41+ cells were observed in *Vcan*$^{Hdf/Hdf}$ yolk sac. The high magnification image shows the distinct cell populations marked by versican and CD41. The white arrowheads mark weak CD41 staining of *Vcan*$^{Hdf/Hdf}$ cells that also lack the rounded morphologies present in the wild-type blood cells (N=3 yolk sacs from each genotype).

(C) Cross section of an E8.5 wild type blood island stained with HAbp (red) and CD41 (green) showing no overlap of HA and CD41+ cells (N=3 yolk sacs).

(D) Methylcellulose colony forming assay shows significantly fewer blood colony forming units (CFUs) *Vcan*$^{Hdf/Hdf}$ yolk sacs and embryos (N=3 yolk sacs and three embryos from each genotype, error bars= S.D.,*, $p<0.05$; **, $p<0.001$).

(E-I) qRT-PCR analysis of wild type and *Vcan*$^{Hdf/Hdf}$ yolk sacs and embryos show significantly lower *Flk1* expression **(E),** but not *Has2* or *Brachyury* **(F)** expression in *Vcan*$^{Hdf/Hdf}$ mutants. **(G)** CD41 *(Itga2b)* and *Runx1* expression were significantly lower in *Vcan*$^{Hdf/Hdf}$ yolk yolk sac and embryos. **(H)** Blood markers *β-globin*, *Gata1* and CD45 (*Ptprc*) and the vascular endothelial

marker CD31 (*Pecam1*) **(l)**, were reduced in *Vcan*$^{Hdf/Hdf}$ yolk sacs and embryos (N=3 yolk sacs and three embryos from each genotype, error bars= S.E.M;*, $p<0.05$; **, $p<0.01$; ***, $p<0.001$).

Figure 4

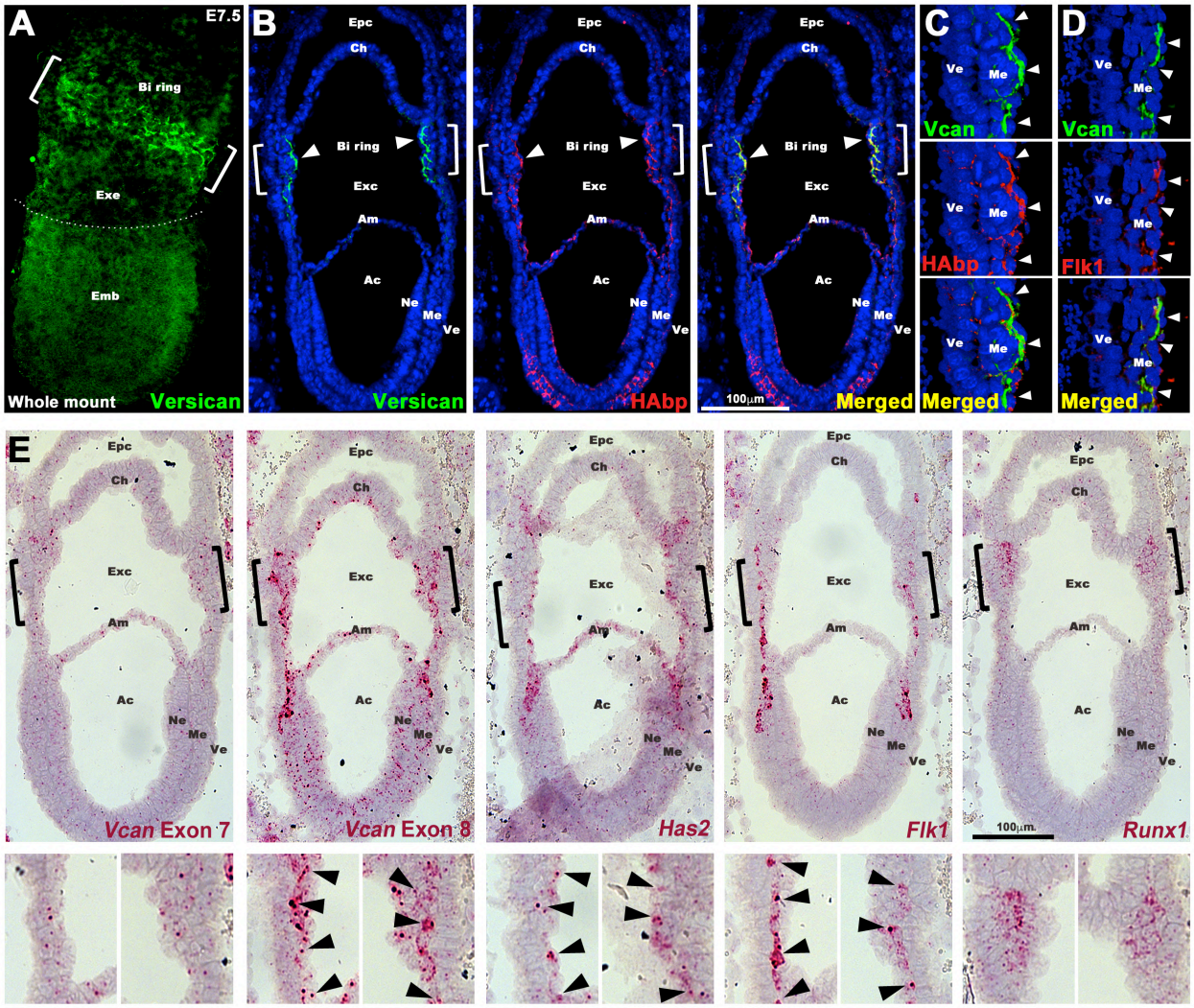

Figure 4. Versican and HA distribution co-localizes with Flk1+ cells from their origin at gastrulation.

(A) Maximum intensity projection image of an E7.5 embryo shows strong versican staining (green) in the putative blood island (BI) ring (white brackets) located in the proximal extraembryonic (Exe) region. Emb, embryo

(B-E) Serial sections of E7.5 wild type embryos analyzed by immunostaining **(B-D)**, or by RNA in situ hybridization **(E)**. **(B-C)** Versican (green) and HAbp (red) colocalize in extraembryonic mesoderm corresponding to the blood island ring (white brackets and arrowheads). The blood islands on the left are shown at high magnification in **(C-D)**. Arrowheads show colocalization of

versican, HAbp and Flk1 in extraembryonic mesoderm (N=4 embryos). Epc, ectoplacental cavity; Ch, chorion; Exc, exocelomic cavity; Am, amnion; Ac, amnion cavity; Ne, neural ectoderm; Me, mesoderm; Ve, visceral endoderm.

(E) *In situ* hybridization for *Vcan* exon 7, *Vcan* exon 8, *Has2*, *Flk1* and *Runx1*. *Vcan* exon 8, *Has2* and *Flk1* mRNAs have near-identical expression patterns (red) corresponding to primitive streak cells migrating towards the extra-embryonic mesoderm. *Vcan* exon 7 (GAGα) shows less intense expression, but also overlaps. *Runx1* marks committed blood cells (N=4 embryos). Scale bars in **B,E**= 100μm.

Figure 5

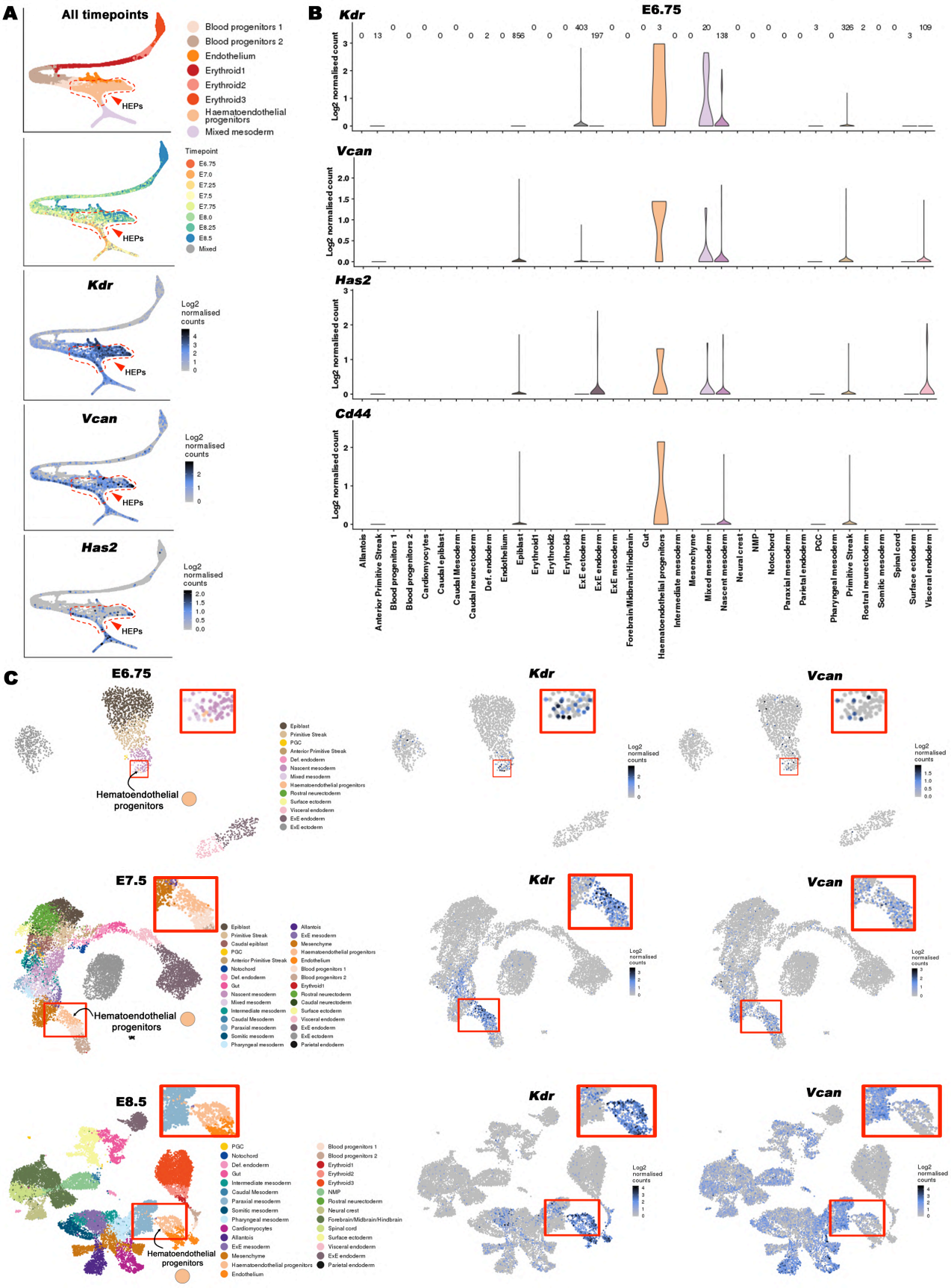
A
All timepoints
Blood progenitors 1
Blood progenitors 2
Endothelium
Erythroid1
Erythroid2
Erythroid3
Haematoendothelial progenitors
Mixed mesoderm
HEPs
Timepoint
E6.75
E7.0
E7.25
E7.5
E7.75
E8.0
E8.25
E8.5
Mixed
Kdr
Vcan
Has2
Log2 normalised counts
B
E6.75
Kdr
Vcan
Has2
Cd44
Log2 normalised count
Allantois
Anterior Primitive Streak
Blood progenitors 1
Blood progenitors 2
Cardiomyocytes
Caudal epiblast
Caudal Mesoderm
Caudal neurectoderm
Def. endoderm
Endothelium
Epiblast
Erythroid1
Erythroid2
Erythroid3
ExE ectoderm
ExE endoderm
ExE mesoderm
Forebrain/Midbrain/Hindbrain
Gut
Haematoendothelial progenitors
Intermediate mesoderm
Mesenchyme
Mixed mesoderm
Nascent mesoderm
Neural crest
NMP
Notochord
Paraxial mesoderm
Parietal endoderm
PGC
Pharyngeal mesoderm
Primitive Streak
Rostral neurectoderm
Somitic mesoderm
Spinal cord
Surface ectoderm
Visceral endoderm
C
E6.75
Kdr
Vcan
Hematoendothelial progenitors
E7.5
E8.5

Figure 5. A single cell RNA transcriptome atlas of mouse gastrulation illustrates specific expression of Vcan and Has2 by Kdr-expressing hemato-endothelial cells.

(A) Force-directed graph layout of blood-related lineages showing the lineage-specific and time-resolved expression of *Kdr, Vcan* and *Has2*. The stippled red line encircles hemato-endothelial progenitors.

(B) Violin plots of *Kdr, Vcan*, Has2 and *Cd44* expression by individual cells of various lineages from E6.75 embryos. Note strong co-expression of these genes by single hemato-endothelial progenitors.

(C) Uniform manifold approximation and projection (UMAP) plots showing overlap between *Kdr* and *Vcan* expression at different gestational ages. High magnification inserts of the hemato-endothelial progenitors are indicated within red boxes.

Figure 6

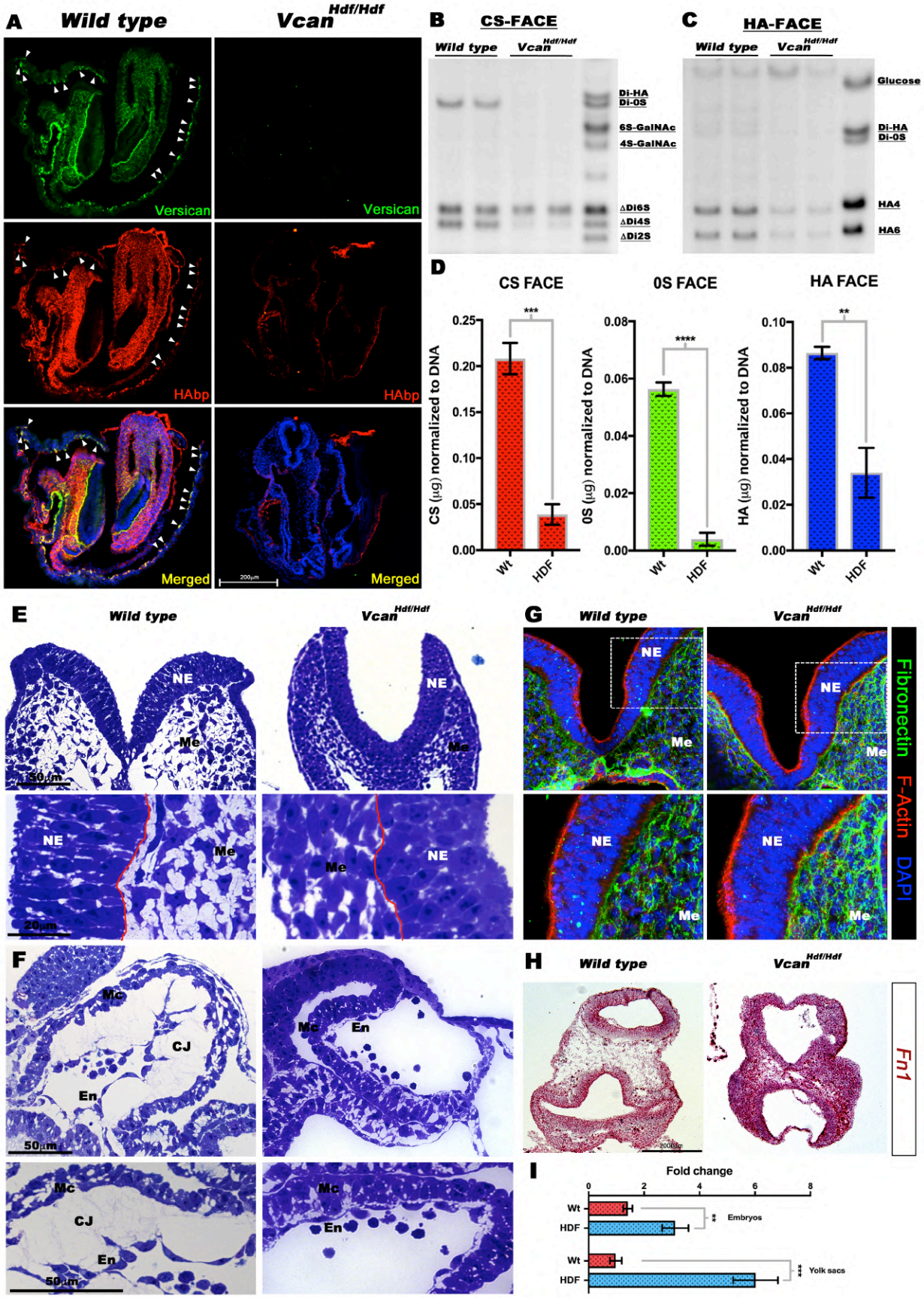
A
Wild type
Vcan Hdf/Hdf
Versican
HAbp
Merged
200µm
B
CS-FACE
Wild type
Vcan Hdf/Hdf
Di-HA
Di-0S
6S-GalNAc
4S-GalNAc
ΔDi6S
ΔDi4S
ΔDi2S
C
HA-FACE
Glucose
HA4
HA6
D
CS FACE
0S FACE
HA FACE
CS (µg) normalized to DNA
0S (µg) normalized to DNA
HA (µg) normalized to DNA
Wt
HDF
E
NE
Me
150µm
20µm
F
Mc
CJ
En
50µm
G
Fibronectin
F-Actin
DAPI
H
Fn1
200µm
I
Fold change
Embryos
Yolk sacs

Figure 6. *Vcan* inactivation results in a loss of hyaluronan.

(A) Versican (green) and HAbp (red) staining of E8.5 wild type and *Vcan*$^{Hdf/Hdf}$ embryos shows severe reduction of HAbp staining in the absence of versican. White arrowheads indicate versican and HAbp-stained yolk sac blood islands.

(B-D) Fluorophore-assisted carbohydrate electrophoresis (FACE) analysis for chondroitin sulfate **(B)** and hyaluronan **(C)** in E8.5 littermate embryos.

Note that versican is the major chondroitin sulfate proteoglycan in E8.5 embryos.

(C) Hyaluronan is significantly reduced in *Vcan*$^{Hdf/Hdf}$ embryos. **(D)** Quantification of chondroitin sulfate and hyaluronan detected by FACE, normalized to DNA (n=4 embryos from each genotype, error bars= S.E.M.,**, $p<0.01$; ***, $p<0.001$; ****, $p<0.0001$).

(E-F) 1 μm thick, toluidine blue-stained Eponate 12 sections from E8.5 wild type and *Vcan*$^{Hdf/Hdf}$ embryos show compaction of mesenchymal cells (Me) in craniofacial mesoderm **(E)** and loss of cardiac jelly (CJ) formation **(F)** between the myocardium (Mc) and endocardium (En). The red line indicates the boundary of the neural epithelium (NE) and mesenchyme.

(G) E8.5 wild *Vcan*$^{Hdf/Hdf}$ embryo sections stained with F-actin (red) and fibronectin (green) show increased fibronectin staining.

(H-I) *In situ* hybridization **(H)** and qRT-PCR **(I)** for *Fn1* shows increased transcription in *Vcan*$^{Hdf/Hdf}$ embryos and yolk sacs (n=3 embryos and yolk sacs from each genotype, error bars= S.E.M.;**, $p<0.01$; ***, $p<0.0001$). Scale bar in **A**= 200μm, 50μm and 20μm in E, 50μm in **F** and 200μm in **H**.

Figure 7

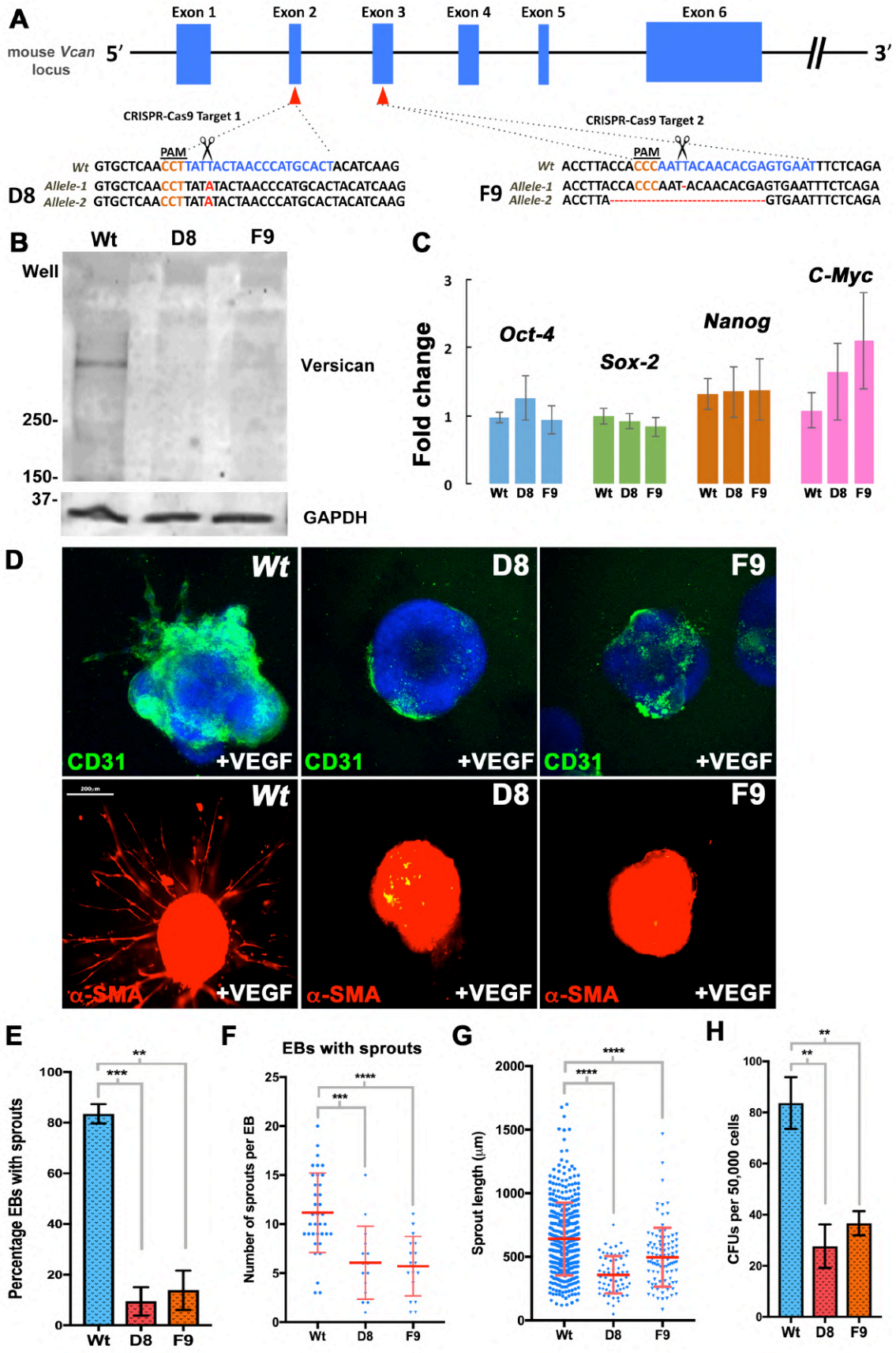
A
mouse Vcan locus
5′
3′
Exon 1
Exon 2
Exon 3
Exon 4
Exon 5
Exon 6
CRISPR-Cas9 Target 1
CRISPR-Cas9 Target 2
PAM
Wt GTGCTCAACCTTATTACTAACCCATGCACTACATCAAG
D8 Allele-1 GTGCTCAACCTTATATACTAACCCATGCACTACATCAAG
Allele-2 GTGCTCAACCTTATATACTAACCCATGCACTACATCAAG
Wt ACCTTACCACCCAATTACAACACGAGTGAATTTCTCAGA
F9 Allele-1 ACCTTACCACCCAAT-ACAACACGAGTGAATTTCTCAGA
Allele-2 ACCTTA----------GTGAATTTCTCAGA
B
Wt
D8
F9
Well
250-
150-
37-
Versican
GAPDH
C
Fold change
Oct-4
Sox-2
Nanog
C-Myc
Wt D8 F9
D
Wt
D8
F9
CD31
+VEGF
α-SMA
E
Percentage EBs with sprouts
F
EBs with sprouts
Number of sprouts per EB
G
Sprout length (μm)
H
CFUs per 50,000 cells

Figure 7. Embryoid bodies (EBs) from *Vcan*-null mouse embryonic stem cells (mESCs) are unresponsive to VEGF and form few blood colonies.

(A) Partial *Vcan* locus showing targeting by independent guide RNAs (gRNAs) targeting exon 2 and exon 3. Black scissors indicate the expected Cas9 cleavage site 3 bp from the protospacer adjacent motif (PAM, orange lettering). An exon 2 mutant mESC clone (D8) had a homozygous 1 bp insertion (bold red letters) and an exon 3 mutant mESC clone (F9) had heterozygous targeting: deletion of T/A in one allele and a deletion of 19 bp in the other. Each mutation resulted in a frame shift and truncated the reading frame.

(B) Versican western blot from 10-day differentiated EBs shows lack of versican in *Vcan* EBs derived from mutant clones D8 and F9.

(C) qRT-PCR analysis showing that expression of pluripotency markers *Oct4*, *Sox2*, *Nanog* and *C-myc* in D8 and F9 was unaffected by gene editing (N=3 independent batches of EBs from each genotype, error bars= S.E.).

(D) 4-day-old *Vcan*-null embryoid bodies embedded in collagen I and treated with $VEGF_{165}$ for 12 days lack vascular sprouting identified by CD31 (green) or α-SMA (red) immunostaining (N=3 independent batches of EBs from each genotype).

(E) D8 and F9 EBs show significantly fewer vascular sprouts (N=3 independent batches of EBs from each genotype, error bars= S.E. **, $p<0.01$; ***, $p<0.001$).

(F) Quantification of the number of sprouts per EB in wild type, D8 and F9 EBs show significantly fewer in *Vcan* null lines (N=3 independent batches of EBs from each genotype, error bars= S.D. ***, $p<0.001$; ****, $p<0.0001$).

(G) Quantification of vascular sprout length in EBs with sprouts in wild type, D8 and F9 EBs shows significantly shorter sprouts in *Vcan* null lines (N=3 independent batches of EBs from each genotype, error bars= S.D. ****, $p<0.0001$).

(H) Methylcellulose colony formation assay using dissociated 10-day old EBs shows significantly fewer blood progenitors in *Vcan* null EBs. N=3 independent experiments (N=3

independent batches of EBs from each genotype, error bars= S.D. **, $p<0.01$). Scale bar in D is 200 μm.

References:

Asano, K., Nelson, C.M., Nandadasa, S., Aramaki-Hattori, N., Lindner, D.J., Alban, T., Inagaki, J., Ohtsuki, T., Oohashi, T., Apte, S.S.*, et al.* (2017). Stromal Versican Regulates Tumor Growth by Promoting Angiogenesis. Sci Rep *7*, 17225.

Baker, M., Robinson, S.D., Lechertier, T., Barber, P.R., Tavora, B., D'Amico, G., Jones, D.T., Vojnovic, B., and Hodivala-Dilke, K. (2012). Use of the mouse aortic ring assay to study angiogenesis. Nat Protoc *7*, 89-104.

Bode-Lesniewska, B., Dours-Zimmermann, M.T., Odermatt, B.F., Briner, J., Heitz, P.U., and Zimmermann, D.R. (1996). Distribution of the large aggregating proteoglycan versican in adult human tissues. J Histochem Cytochem *44*, 303-312.

Burns, T.A., Dours-Zimmermann, M.T., Zimmermann, D.R., Krug, E.L., Comte-Walters, S., Reyes, L., Davis, M.A., Schey, K.L., Schwacke, J.H., Kern, C.B.*, et al.* (2014). Imbalanced expression of Vcan mRNA splice form proteins alters heart morphology and cellular protein profiles. PLoS One *9*, e89133.

Buschmann, M.D., and Grodzinsky, A.J. (1995). A molecular model of proteoglycan-associated electrostatic forces in cartilage mechanics. J Biomech Eng *117*, 179-192.

Calabro, A., Benavides, M., Tammi, M., Hascall, V.C., and Midura, R.J. (2000a). Microanalysis of enzyme digests of hyaluronan and chondroitin/dermatan sulfate by fluorophore-assisted carbohydrate electrophoresis (FACE). Glycobiology *10*, 273-281.

Calabro, A., Hascall, V.C., and Midura, R.J. (2000b). Adaptation of FACE methodology for microanalysis of total hyaluronan and chondroitin sulfate composition from cartilage. Glycobiology *10*, 283-293.

Camenisch, T.D., Spicer, A.P., Brehm-Gibson, T., Biesterfeldt, J., Augustine, M.L., Calabro, A., Jr., Kubalak, S., Klewer, S.E., and McDonald, J.A. (2000). Disruption of hyaluronan synthase-2 abrogates normal cardiac morphogenesis and hyaluronan-mediated transformation of epithelium to mesenchyme. J Clin Invest *106*, 349-360.

Doudna, J.A., and Charpentier, E. (2014). Genome editing. The new frontier of genome engineering with CRISPR-Cas9. Science *346*, 1258096.

Dours-Zimmermann, M.T., Maurer, K., Rauch, U., Stoffel, W., Fassler, R., and Zimmermann, D.R. (2009). Versican V2 assembles the extracellular matrix surrounding the nodes of ranvier in the CNS. J Neurosci *29*, 7731-7742.

Dours-Zimmermann, M.T., and Zimmermann, D.R. (1994). A novel glycosaminoglycan attachment domain identified in two alternative splice variants of human versican. J Biol Chem *269*, 32992-32998.

Dzierzak, E., and Speck, N.A. (2008). Of lineage and legacy: the development of mammalian hematopoietic stem cells. Nat Immunol *9*, 129-136.

Evanko, S.P., Angello, J.C., and Wight, T.N. (1999). Formation of hyaluronan- and versican-rich pericellular matrix is required for proliferation and migration of vascular smooth muscle cells. Arterioscler Thromb Vasc Biol *19*, 1004-1013.

Evanko, S.P., Tammi, M.I., Tammi, R.H., and Wight, T.N. (2007). Hyaluronan-dependent pericellular matrix. Adv Drug Deliv Rev *59*, 1351-1365.

Ferkowicz, M.J., Starr, M., Xie, X., Li, W., Johnson, S.A., Shelley, W.C., Morrison, P.R., and Yoder, M.C. (2003). CD41 expression defines the onset of primitive and definitive hematopoiesis in the murine embryo. Development *130*, 4393-4403.

Ferkowicz, M.J., and Yoder, M.C. (2005). Blood island formation: longstanding observations and modern interpretations. Exp Hematol *33*, 1041-1047.

Francis, S.E., Goh, K.L., Hodivala-Dilke, K., Bader, B.L., Stark, M., Davidson, D., and Hynes, R.O. (2002). Central roles of alpha5beta1 integrin and fibronectin in vascular development in mouse embryos and embryoid bodies. Arterioscler Thromb Vasc Biol *22*, 927-933.

George, E.L., Georges-Labouesse, E.N., Patel-King, R.S., Rayburn, H., and Hynes, R.O. (1993). Defects in mesoderm, neural tube and vascular development in mouse embryos lacking fibronectin. Development *119*, 1079-1091.
Gu, Y., Runyan, C., Shoemaker, A., Surani, A., and Wylie, C. (2009). Steel factor controls primordial germ cell survival and motility from the time of their specification in the allantois, and provides a continuous niche throughout their migration. Development *136*, 1295-1303.
Hattori, N., Carrino, D.A., Lauer, M.E., Vasanji, A., Wylie, J.D., Nelson, C.M., and Apte, S.S. (2011). Pericellular versican regulates the fibroblast-myofibroblast transition: a role for ADAMTS5 protease-mediated proteolysis. J Biol Chem *286*, 34298-34310.
Hope, C., Foulcer, S., Jagodinsky, J., Chen, S.X., Jensen, J.L., Patel, S., Leith, C., Maroulakou, I., Callander, N., Miyamoto, S.*, et al.* (2016). Immunoregulatory roles of versican proteolysis in the myeloma microenvironment. Blood *128*, 680-685.
Hunziker, E.B., Herrmann, W., and Schenk, R.K. (1983). Ruthenium hexammine trichloride (RHT)-mediated interaction between plasmalemmal components and pericellular matrix proteoglycans is responsible for the preservation of chondrocytic plasma membranes in situ during cartilage fixation. J Histochem Cytochem *31*, 717-727.
Jinek, M., Chylinski, K., Fonfara, I., Hauer, M., Doudna, J.A., and Charpentier, E. (2012). A programmable dual-RNA-guided DNA endonuclease in adaptive bacterial immunity. Science *337*, 816-821.
Kimata, K., Oike, Y., Tani, K., Shinomura, T., Yamagata, M., Uritani, M., and Suzuki, S. (1986). A large chondroitin sulfate proteoglycan (PG-M) synthesized before chondrogenesis in the limb bud of chick embryo. J Biol Chem *261*, 13517-13525.
Kloeckener-Gruissem, B., Bartholdi, D., Abdou, M.T., Zimmermann, D.R., and Berger, W. (2006). Identification of the genetic defect in the original Wagner syndrome family. Mol Vis *12*, 350-355.
Kloeckener-Gruissem, B., Neidhardt, J., Magyar, I., Plauchu, H., Zech, J.C., Morle, L., Palmer-Smith, S.M., Macdonald, M.J., Nas, V., Fry, A.E.*, et al.* (2013). Novel VCAN mutations and evidence for unbalanced alternative splicing in the pathogenesis of Wagner syndrome. Eur J Hum Genet *21*, 352-356.
Le Jan, S., Hayashi, M., Kasza, Z., Eriksson, I., Bishop, J.R., Weibrecht, I., Heldin, J., Holmborn, K., Jakobsson, L., Soderberg, O.*, et al.* (2012). Functional overlap between chondroitin and heparan sulfate proteoglycans during VEGF-induced sprouting angiogenesis. Arterioscler Thromb Vasc Biol *32*, 1255-1263.
McCulloch, D.R., Nelson, C.M., Dixon, L.J., Silver, D.L., Wylie, J.D., Lindner, V., Sasaki, T., Cooley, M.A., Argraves, W.S., and Apte, S.S. (2009). ADAMTS metalloproteases generate active versican fragments that regulate interdigital web regression. Dev Cell *17*, 687-698.
Mead, T.J., Du, Y., Nelson, C.M., Gueye, N.A., Drazba, J., Dancevic, C.M., Vankemmelbeke, M., Buttle, D.J., and Apte, S.S. (2018). ADAMTS9-Regulated Pericellular Matrix Dynamics Governs Focal Adhesion-Dependent Smooth Muscle Differentiation. Cell Rep *23*, 485-498.
Midura, R.J., Cali, V., Lauer, M.E., Calabro, A., and Hascall, V.C. (2018). Quantification of hyaluronan (HA) using a simplified fluorophore-assisted carbohydrate electrophoresis (FACE) procedure. Methods Cell Biol *143*, 297-316.
Mjaatvedt, C.H., Yamamura, H., Capehart, A.A., Turner, D., and Markwald, R.R. (1998). The Cspg2 gene, disrupted in the hdf mutant, is required for right cardiac chamber and endocardial cushion formation. Dev Biol *202*, 56-66.
Nagy, A., Rossant, J., Nagy, R., Abramow-Newerly, W., and Roder, J.C. (1993). Derivation of completely cell culture-derived mice from early-passage embryonic stem cells. Proc Natl Acad Sci U S A *90*, 8424-8428.
Nandadasa, S., Foulcer, S., and Apte, S.S. (2014). The multiple, complex roles of versican and its proteolytic turnover by ADAMTS proteases during embryogenesis. Matrix Biol *35*, 34-41.

Nandadasa, S., Nelson, C.M., and Apte, S.S. (2015). ADAMTS9-Mediated Extracellular Matrix Dynamics Regulates Umbilical Cord Vascular Smooth Muscle Differentiation and Rotation. Cell Rep *11*, 1519-1528.
Oladipupo, S.S., Kabir, A.U., Smith, C., Choi, K., and Ornitz, D.M. (2018). Impaired tumor growth and angiogenesis in mice heterozygous for Vegfr2 (Flk1). Sci Rep *8*, 14724.
Perris, R., Perissinotto, D., Pettway, Z., Bronner-Fraser, M., Morgelin, M., and Kimata, K. (1996). Inhibitory effects of PG-H/aggrecan and PG-M/versican on avian neural crest cell migration. Faseb J *10*, 293-301.
Pijuan-Sala, B., Griffiths, J.A., Guibentif, C., Hiscock, T.W., Jawaid, W., Calero-Nieto, F.J., Mulas, C., Ibarra-Soria, X., Tyser, R.C.V., Ho, D.L.L.*, et al.* (2019). A single-cell molecular map of mouse gastrulation and early organogenesis. Nature *566*, 490-495.
Protin, U., Schweighoffer, T., Jochum, W., and Hilberg, F. (1999). CD44-deficient mice develop normally with changes in subpopulations and recirculation of lymphocyte subsets. J Immunol *163*, 4917-4923.
Red-Horse, K., Crawford, Y., Shojaei, F., and Ferrara, N. (2007). Endothelium-microenvironment interactions in the developing embryo and in the adult. Dev Cell *12*, 181-194.
Risau, W., and Flamme, I. (1995). Vasculogenesis. Annu Rev Cell Dev Biol *11*, 73-91.
Rothschild, P.R., Audo, I., Nedelec, B., Ghiotti, T., Brezin, A.P., Monin, C., and Valleix, S. (2013). De novo splice mutation in the versican gene in a family with Wagner syndrome. JAMA Ophthalmol *131*, 805-807.
Shalaby, F., Ho, J., Stanford, W.L., Fischer, K.D., Schuh, A.C., Schwartz, L., Bernstein, A., and Rossant, J. (1997). A requirement for Flk1 in primitive and definitive hematopoiesis and vasculogenesis. Cell *89*, 981-990.
Shinomura, T., Nishida, Y., Ito, K., and Kimata, K. (1993). cDNA cloning of PG-M, a large chondroitin sulfate proteoglycan expressed during chondrogenesis in chick limb buds. Alternative spliced multiforms of PG-M and their relationships to versican. J Biol Chem *268*, 14461-14469.
Suwan, K., Choocheep, K., Hatano, S., Kongtawelert, P., Kimata, K., and Watanabe, H. (2009). Versican/PG-M Assembles Hyaluronan into Extracellular Matrix and Inhibits CD44-mediated Signaling toward Premature Senescence in Embryonic Fibroblasts. J Biol Chem *284*, 8596-8604.
Szabo, A., Melchionda, M., Nastasi, G., Woods, M.L., Campo, S., Perris, R., and Mayor, R. (2016). In vivo confinement promotes collective migration of neural crest cells. J Cell Biol *213*, 543-555.
van Wijk, X.M., and van Kuppevelt, T.H. (2014). Heparan sulfate in angiogenesis: a target for therapy. Angiogenesis *17*, 443-462.
Wu, Y.J., La Pierre, D.P., Wu, J., Yee, A.J., and Yang, B.B. (2005). The interaction of versican with its binding partners. Cell Res *15*, 483-494.
Yamagata, M., Suzuki, S., Akiyama, S.K., Yamada, K.M., and Kimata, K. (1989). Regulation of cell-substrate adhesion by proteoglycans immobilized on extracellular substrates. J Biol Chem *264*, 8012-8018.
Yamamura, H., Zhang, M., Markwald, R.R., and Mjaatvedt, C.H. (1997). A heart segmental defect in the anterior-posterior axis of a transgenic mutant mouse. Dev Biol *186*, 58-72.
Zheng, P.S., Wen, J., Ang, L.C., Sheng, W., Viloria-Petit, A., Wang, Y., Wu, Y., Kerbel, R.S., and Yang, B.B. (2004). Versican/PG-M G3 domain promotes tumor growth and angiogenesis. FASEB J *18*, 754-756.
Zimmermann, D.R., and Ruoslahti, E. (1989). Multiple domains of the large fibroblast proteoglycan, versican. Embo J *8*, 2975-2981.

STAR METHODS:

KEY RESOURCES TABLE

REAGENT or RESOURCE	SOURCE	IDENTIFIER
Antibodies		
Hamster monoclonal anti-mouse CD31	Millipore-Sigma	MAB1398Z
Rabbit polyclonal anti-versican	Millipore-Sigma	AB1033
Rabbit polyclonal anti-fibronectin	Abcam	Ab2413
Rabbit polyclonal anti-collagen-IV	Rockland antibodies and assays	600-401-106
Rat monoclonal anti-mouse Flk1 (clone Avas12)	Thermo Fisher	17-5821-81
Rat monoclonal anti-mouse CD41	Biolegend	133904
Mouse monoclonal anti-smooth muscle α-actin	Sigma-Aldrich	C6198
Mouse monoclonal anti-GAPDH	Millipore-Sigma	MAB374
Bacterial and Virus Strains		
One shot TOP10 chemically competent *E. coli* cells	Thermo Fisher	K280020
Biological Samples		
N/A	N/A	N/A
Chemicals, Peptides, and Recombinant Proteins		
Leukemia inhibitory factor (LIF)	EMD-Millipore	ESG1106
Recombinant $VEGF_{165}$	PreproTech	100-20
Bovine type 1 collagen	Corning	354231
Proteus vulgaris chondroitinase ABC	Sigma-Aldrich	3667
Biotinylated hyaluronan binding protein (HAbp)	Millipore-Sigma, Calbiochem	385911
Alexa Fluor-568 phalloidin	Life Technologies	A12380
Ruthenium hexamine trichloride	Sigma-Aldrich	262005
Protease inhibitor cocktail	Roche	11873580001
Critical Commercial Assays		
RNAscope mouse *Vcan* exon 7 (GAG-α)	Advanced Cell Diagnostics	428311
RNAscope mouse *Vcan* exon 8 (GAG-β)	Advanced Cell Diagnostics	428321
RNAscope mouse *Has2*	Advanced Cell Diagnostics	465171
RNAscope mouse *Kdr* (Flk1)	Advanced Cell Diagnostics	414811
RNAscope mouse *Runx1*	Advanced Cell Diagnostics	406671
MethoCult GF M3534	Stem Cell Technologies	03534
Bullseye EvaGreen qPCR mix	MIDSCI	BEQPCR-S
Deposited Data		
N/A	N/A	N/A
Experimental Models: Cell Lines		

R1 mouse embryonic stem cells (mESC)	CWRU Transgenic & Targeting Facility	Nagy A et al., 1993 ATCC, SCRC-1011
Experimental Models: Organisms/Strains		
Mouse: *Vcan*$^{Hdf/+}$: Vcan$^{Tg(Hoxa1)1Chm}$/C57BL/6J		MGI:1857689 Yamamura H, et al., 1997
Oligonucleotides		
See Supplemental Table 1 for qRT-PCR primers	This paper	N/A
Recombinant DNA		
mVcan-E2-U6gRNA-Cas9-2A-GFP	Sigma-Aldrich	target ID MM0000080027
mVcan-E3-U6gRNA-Cas9-2A-GFP	Sigma-Aldrich	target ID MM0000080028
pCR-Blunt II-TOPO	Life Technologies	K2800-40
Software and Algorithms		
LI-COR Image Studio (ver. 4.0)	LI-COR	N/A
Volocity 3D imaging software (ver. 6.3)	PerkinElmer	N/A
Image J	NIH	https://imagej.nih.gov/ij/
Other		
N/A		

Mice

Vcan$^{Tg(Hoxa1)1Chm}$ (refrerred to herein as *Vcan*^{Hdf}) mice (Yamamura et al., 1997) were used under a material transfer agreement from Roche. Mouse experiments were conducted with IACUC approval (Protocols 2015:1530 and 2018:2045). Mice were maintained in a fixed light-dark cycle with food and water *ad libitum*. For genotyping E8.5 embryos with intact yolk sacs, the allantois was dissected out and lysed in 10μl DirectPCR (Tail) digest reagent (Qiagen, catalog no. 102-T) supplemented with 1μl of proteinase K overnight at 55°C. A dissected tailpiece was used to genotype E9.5 embryos. *Vcan*^{Hdf} and wild type alleles were identified with a specific genotyping strategy (Figure S1). *Vcan*$^{Hdf/Hdf}$ embryos were compared to wild type littermates in all experiments.

Mouse embryonic stem cell (mESC) culture.

R1 mESC (Nagy et al., 1993) were cultured on 0.3% type B gelatin (Sigma-Aldrich, catalog no. G9382) coated 60 mm cell culture plates in Iscove's Modified Dulbecco's Medium (IMDM)

containing 4mM L-glutamine and 1mM sodium pyruvate, supplemented with 20% fetal bovine serum (Hyclone, catalog no. SH30071), 0.1 mM cell culture grade 2-mercaptoethanol (Gibco, Life Technologies, catalog no. 21985), 0.1mM nonessential amino acids (Gibco, Life Technologies, catalog no. 11140-050), 50 μg/mL penicillin/streptomycin and $1x10^6$ units/mL leukemia inhibitory factor (LIF; ESGRO, EMD Millipore, catalog no. ESG1106) in a humidified 5% CO_2, 37°C environment. mESC were maintained at 60-80% confluence, with daily medium change and passaged every other day in a 1:5 split.

CRISPR/Cas9 targeting of mESC *Vcan*

2.5 μg of CRISPR/Cas9 plasmids in the U6gRNA-Cas9-2A-GFP vector, targeting *Vcan* exon 2 or exon 3 (Sigma-Aldrich, target IDs MM0000080027 and MM0000080028) were transfected into R1 mESCs at 60-80% confluence in 6-well plates coated with 0.3% gelatin, using FuGene 6 (Promega, catalog no. E2691). 24 hrs post-transfection, individual GFP+ mESCs were sorted into 96-well plates coated with 0.3% gelatin using a FACSAria-II cell sorter (BD Biosciences). Fast-growing wells (containing >1000 cells/well) were trypsinized and expanded to 24-well cell culture plates after 7-10 days. Culture medium was replaced daily. Genomic DNA from clones was isolated using DirectPCR (Tail) reagent (Viagen, catalog no. 102-T) and *Vcan* exon 2 and exon 3 were amplified using Phusion *Taq* (NEB, catalog no. F530L) (see SI). Amplicons were excised from 2% agarose gels, purified using the QIAquick Gel Extraction kit (QIAGEN, catalog no. 28704) and cloned into pCR-Blunt II-TOPO vector using the Zero blunt PCR cloning kit (Life Technologies, Invitrogen, catalog no. K2800-40). Plasmid DNA was harvested from bacterial colonies for Sanger-sequencing to determine the precise mutations. Two independent *Vcan*-null mESC clones, D8 and F9, were established. Western blotting and immunostaining of 10-day old embryoid bodies from these lines (see below) confirmed *Vcan* inactivation.

Immunostaining and fluorescence microscopy

Immunostaining of E9.5 and E8.5 yolk sac was carried out on 30μm thick vibratome sections (Nandadasa et al., 2015) or paraffin-embedded 7 μm sections. Immunostaining of collagen-embedded embryoid bodies were carried out in 4-chamber cell culture slides (Fisher Scientific, catalog no. 354114). Confocal microscopy images of whole mount mouse embryos and sections were acquired using a Leica TCS SP5 II multiphoton confocal microscope equipped with a 25X water immersion objective (Leica Microsystems, Wetzlar, Germany). For 3D-projection of whole mount Z-stacks, the Volocity 3D imaging software was used (version 6.3, PerkinElmer, Inc., Waltham, MA) in maximum intensity projection method. Embryoid body formation and induction of vascular sprouts is described in S.I.

Methylcellulose colony formation assay

Single cell suspensions of E8.5 embryos, yolk sacs or day-10 embryoid bodies (EBs) were generated by incubation with trypsin for 10 minutes followed by disaggregation by pipetting with a 200 μL pipette tip until complete. 50,000 cells from each experimental group were transferred to a single 35 mm culture dish containing 1 mL of MethoCult GF M3534 culture medium (Methylcellulose medium with recombinant cytokines for mouse cells, Stem Cell Technologies, Vancouver, CA, catalog no. 03534) using a 3 mL syringe and 16-gauge needle, following the manufacturer's protocol. Triplicate cultures from each genotype were incubated for 14 days in a humidified, 5% CO_2, 37°C cell culture incubator. Blood colonies were counted using an inverted microscope. Aggregates with >50 cells were considered a colony-forming unit (CFU).

Primary antibodies and dilutions

For staining whole mount embryos, yolk sacs or vibratome sections, the following antibodies, staining reagents and dilutions were used: Rabbit polyclonal anti-mouse versican GAGβ domain (Millipore-Sigma, catalog no. AB1033) 1:200; biotinylated hyaluronan binding protein (HAbp) (Millipore-Sigma, Calbiochem, catalog no. 385911) 1:100; rabbit polyclonal anti-fibronectin (Abcam, catalog no. Ab2413) 1:200; rabbit polyclonal anti-collagen-IV (Rockland antibodies and

assays, catalog no. 600-401-106) 1:400; rat monoclonal anti-mouse Flk1 (clone Avas12, Thermo Fisher, catalog no. 17-5821-81) 1:200; hamster anti-mouse CD31 (Milipore-Sigma, catalog no. MAB1398Z) 1:400; FITC-conjugated anti-mouse CD41 (Biolegend, catalog no.133904) 1:100; mouse monoclonal Cy3 conjugated smooth muscle α-actin (Sigma-Aldrich, catalog no. C6198) 1:600;Alexa Fluor-568 phalloidin (Life Technologies, catalog no. A12380) 1:500. All primary antibodies were diluted in 10% normal goat serum in PBST (PBS+ 0.1% Tween 20) and incubated overnight at 4°C. Alexa488, 568 or 647-conjugated secondary antibodies against the corresponding species, or streptavidin conjugated Alexa488 or 568-labeled antibodies for HAbp detection were purchased from Invitrogen and were used at 1:400 dilution at room temperature for 2-3hrs. Slides were photographed using an Olympus BX51 upright microscope (Olympus, Center Valley, PA) connected to a Leica DFC7000T camera and Leica Application Suite v4.6 imaging software (both from Leica, Wetzlar, Germany).

Quantitative real time RT-PCR (qRT-PCR) analysis

RNA from whole embryos, dissected yolk sacs or EBs was extracted using TRIzol reagent (ThermoFisher Scientific, catalog no. 15596026) according to manufacturer recommendations. 2 μg of RNA from each sample (embryo, yolk sac or EB pool) was used for cDNA synthesis using the high capacity cDNA synthesis kit (Applied Biosystems, Thermo Fisher Scientific, catalog no. 4368814). qRT-PCR was carried out using a CFX96 Touch Real-Time PCR detection system (Bio-Rad Laboratories) with the Bullseye EvaGreen qPCR mix (MIDSCI, catalog no. BEQPCR-S), using primer pairs listed in the Supplemental Table. 18s ribosomal RNA or *Actb* RNA were used for normalization and relative expression of genes was calculated by the $\Delta\Delta$Ct quantification method. An unpaired, two-tailed Student t-test was used to determine statistical significance.

RNAscope *In-situ* hybridization and RNAseq database mining

4% PFA fixed mouse embryos and yolk sacs were paraffin embedded and 7 μm thick sections were collected immediately prior to in-situ hybridization. All RNAscope in situ probes and reagents were from Advanced Cell Diagnostics. The probes were: *Vcan* exon 7 (GAG-α) (catalog no. 428311), *Vcan* exon 8 (GAG-β) (catalog no. 428321), *Has2* (catalog no. 465171), *Flk1 (Kdr)* (catalog no. 414811) and *Runx1* (catalog no. 406671). In situ hybridization was carried out following the user manual for RNAScope 2.5 HD Red detection kit using the RNAscope HybEZ oven. Slides were photographed as described above.

A database containing recent analysis of 116,312 single cells (Pijuan-Sala B, et al., 2019) obtained from gastrulating mouse embryos spanning E6.5 to E8.5 was searched at specific gestational ages for expression of *Vcan, Kdr, Has2* and *Cd44*. Individual data panels were generated by the web portal for the deposited scRNAseq data: https://marionilab.cruk.cam.ac.uk/MouseGastrulation2018/

Western blotting

7.5% reducing SDS-PAGE was used for western blotting. Embryoid bodies were lysed in PBS containing 1% Tween 20 supplemented with a protease inhibitor cocktail (Roche, catalog no. 11873580001). Supernatants obtained after centrifugation at 1200 rpm for 10 minutes were treated with BSA free *Proteus vulgaris* chondroitinase ABC (Sigma-Aldrich, catalog no. 3667) for 2 h at 37°C. Samples were boiled in Laemmli sample buffer (0.375% mM Tris.HCL, 9% SDS, 50% glycerol, 0.03% bromophenol blue, with 9% (v/v) β-mercaptoethanol) for 10 minutes followed by SDS-PAGE. Nitrocellulose membranes with transferred proteins were blocked in LI-COR Odyssey PBS blocking buffer (LI-COR Biosciences, Lincoln, NE catalog no. 927-40000) for 30 minutes in RT. Primary antibodies rabbit anti-mouse versican (GAGβ) antibody (1:1000) (Millipore-Sigma, catalog no. AB1033) or mouse monoclonal GAPDH antibody (1:5000) (Millipore-Sigma, catalog no. MAB374) were diluted in blocking buffer and incubated overnight

at 4°C with gentle rocking. LI-COR IR dye secondary antibodies against mouse and rabbit antibodies (LI-COR Biosciences, Lincoln, NE) were used at 1:10000 dilutions in PBS to detect primary antibodies. A LI-COR Odyssey CLx scanner and the LI-COR Image Studio (ver. 4.0) was used to image western blots.

Fluorophore-assisted carbohydrate electrophoresis

FACE procedures used were essentially as previously published (Calabro et al., 2000a; Calabro et al., 2000b; Midura et al., 2018). In brief, tissue was extensively digested with proteinase K and released glycosaminoglycans (GAGs) were isolated by ice-cold ethanol precipitation and centrifugation. GAGs were resuspended in 0.1 M ammonium acetate, pH 7.0 and then digested overnight with *Streptomyces* hyaluronidase (200 mU) at 37° C for HA-FACE. HA digestion products were separated from other intact GAGs using ice-cold ethanol precipitation and centrifugation. The supernatant was then dried under vacuum centrifugation and reacted with 6.25 mM 2-aminoacridone (AMAC) and 625 mM sodium cyanoborohydride ($NaBH_3CN$) overnight at 37° C. The pellet was resuspended in 0.1 M ammonium acetate, pH 7.0 and then digested overnight with chondroitinase ABC (25 mU) at 37° C fro CS-FACE. CS digestion products were separated from other intact GAGs using ice-cold ethanol precipitation and centrifugation. The supernatant was then dried under vacuum centrifugation and reacted with 6.25 mM AMAC and 625 mM $NaBH_3CN$ overnight at 37° C. AMAC-labeled HA and CS digestion products were loaded onto 20% (w/v) acrylamide gels and these products were resolved by electrophoresis at 500 V constant current over a 50-60 minute run time. FACE gels were imaged while still housed in the gel plates on a UVP ChemiDoc-It^2 515 system. Digital gel images were analyzed for AMAC-labeled HA and CS digestion product band intensities using ImageJ (NIH, Bethesda MD).

Transmission electron microscopy

E9.5 yolk sacs were harvested from timed pregnancies and fixed in 4% PFA + 2.5% glutaraldehyde in PBS overnight. Samples were dehydrated in an ethanol:PBS gradient and

fully dehydrated samples were embedded in pure Eponate12 resin and allowed to polymerize overnight. Ultrathin sections (85 nm) were stained with uranyl acetate and lead citrate and viewed and imaged on a FEI Tecnai G2 Spirit BioTWIN Transmission Electron Microscope (FEI company, Hillsboro, OR) equipped with an Orius 832 CCD camera (Gatan, Inc., Pleasanton, CA).

Some E8.5 embryos were fixed in 4% PFA + 2.5% glutaraldehyde + 0.7% w/v ruthenium hexamine trichloride (Sigma-Aldrich, catalog no. 262005) in PBS overnight to optimize proteoglycan and cell membrane preservation (Hunziker et al., 1983) and embedded in Eponate 12 resin as described above. 1 micron thick sections were stained with 1% toluidine blue containing 2% sodium borate for 30 seconds on a hot plate and washed with distilled water. Slides were mounted with Cytoseal XYL mounting media (ThermoFisher Scientific, catalog no. 22-050-262) and imaged as described for routine microscopy.

Embryoid body formation and $VEGF_{165}$ induced angiogenic-sprouting

mESCs were cultured for two days till 100% confluent, gently washed with PBS and incubated with IMDM without LIF for an additional 48 h. IMDM without LIF was used in subsequent manipulations to form EBs. The medium was removed and 250μl of trypsin was added to each plate and aspirated out after a 30 second incubation leaving a thin film of trypsin. Upon detachment and rounding of cells, 1 mL of IMDM was added to each plate, and a small pipette tip was used to generate small aggregates mechanically from the mESC sheet. The aggregates were transferred to 60 mm (non-adhesive) bacteriological dishes (Corning, catalog no. 351007) containing 5 mL of IMDM, where most curled and formed free-floating spheroids after 24 hrs. These 1-day EBs were transferred to a fresh bacteriological dish with 5 mL of IMDM and cultured for an additional 3 days. 10-20 4-day old EBs from each genotype were transferred to a 4-well chamber (Fisher Scientific, catalog no. 354114) and embedded in bovine type 1 collagen (Corning, catalog no. 354231) containing 30 ng/mL recombinant $VEGF_{165}$ (PreproTech, catalog no. 100-20). 500 μL IMDM containing 30 ng/mL recombinant $VEGF_{165}$, was added atop each

collagen gel and replaced very 4 days for a further 12 days. The collagen-embedded EBs were washed with PBS and fixed in 4% PFA for 15 min, permeabilized by three washes in PBS containing 0.3% Tween 20 for 30 minutes prior to immunostaining with anti-CD31 or anti-smooth muscle α-actin (SMA). For qRT-PCR, EBs in floating culture were incubated for 10 days (day-10 EBs). 300 μL of TRIzol reagent (ThermoFisher scientific, catalog no. 15596026) was used to harvest total RNA from each 60 mm plate.

Embryoid body vascular sprout quantifications

For quantifying EB vascular sprouts, collagen-embedded, fixed embryoid bodies in 4-chamber slides were imaged using an inverted bright field microscope. Images were analyzed by Image J-FIJI (NIH, Bethesda, MD), and the freehand drawing tool was used to trace the length of individual vascular sprouts. A total N= 72 wild type, 68 D8 and 68 F9 EBs were analyzed in 3 independent experiments. Lengths of 402 sprouts from wild type, 91 from D8 and 97 from F9 EBs were measured.